Master's thesis
Astronomy

What kind of data would ascertain real periodicity in the terrestrial impact crater record

Joonas Lyytinen

2008

Tutor: dos. Lauri Jetsu
Censors: dos. Karri Muinonen and dos. Lauri Jetsu

University of Helsinki
Department of Astronomy
P.O. Box 14 (Tähtitorninmäki)
FIN-00014 University of Helsinki

HELSINGIN YLIOPISTO — HELSINGFORS UNIVERSITET — UNIVERSITY OF HELSINKI

Tiedekunta/Osasto — Fakultet/Sektion — Faculty	Laitos — Institution — Department
Matemaattis-luonnontieteellinen	Tähtitieteen laitos

Tekijä — Författare — Author
Joonas Lyytinen

Työn nimi — Arbetets titel — Title

What kind of data would ascertain real periodicity in the terrestrial impact crater record

Oppiaine — Läroämne — Subject
Tähtitiede

Työn laji — Arbetets art — Level	Aika — Datum — Month and year	Sivumäärä — Sidoantal — Number of pages
pro gradu -työ	maaliskuu 2008	51

Tiivistelmä — Referat — Abstract

The possible presence of periodicity in the terrestrial impact crater data has been discussed in several papers since 1984. The authenticity of this detected periodicity data is controversial. It is possible, however, that real periodicity is present and could be detected from more accurate and complete data.

In our study we created simulated different probability distributions for terrestrial impact crater record, that covered completely aperiodic and periodic impact cratering scenarios, as well as two specific combinations of these two cases, with four different impact crater age uncertainties. From these distributions we then generated simulated time series of impact craters with different numbers of craters and tested if the periodicity in the distribution could be detected using the Rayleigh method.

Our analysis shows that if only one third of the terrestrial impact craters are caused by periodic cratering events, the detection of a real period in the data is very difficult and probably could not be detected even if better impact crater data became available. If two thirds of the craters are caused by periodic impacts, detection is possible, but would require substantially better data than which is currently available. We conclude that the periodicities reported so far in the impact crater data are not caused by real physical phenomena.

Maan törmäyskraaterien ikäjakauman mahdollinen ajallinen jaksollisuus on herättänyt laajaa keskustelua sen jälkeen, kun ilmiö ensimmäistä kertaa raportoitiin joukossa arvostettuja tieteellisiä artikkeleita vuonna 1984. Vaikka nykytiedon valossa on kyseenalaista perustuuko havaittu jaksollisuus todelliseen fysikaaliseen ilmiöön, on kuitenkin mahdollista, että jaksollisuus on todella olemassa ja se voitaisiin havaita laajemmalla ja tarkemmalla törmäyskraateriaineistolla.

Tutkimuksessa luotiin simuloidut kraaterien ajalliset tiheys- ja kertymäfunktiot tapauksille, jossa kraaterit syntyvät joko täysin jaksollisella tai satunnaisella prosessilla. Näiden kahden ääritapauksen lisäksi luotiin jakaumat myös kahdelle niiden yhdistelmälle. Nämä mallit mahdollistavat myös erilaisten kraaterien iänmäärityksen epätarkkuuksien huomioonottamisen. Näistä jakaumista luotiin eri pituisia simuloituja kraaterien ikien aikasarjoja. Lopulta simuloiduista aikasarjoista pyrittiin Rayleigh'n menetelmän avulla etsimään jakaumassa ollutta jaksollisuutta.

Tutkimuksemme perusteella ajallisen jaksollisuuden havaitseminen kraateriaikasarjoista on lähes mahdotonta mikäli vain yksi kolmasosa kraatereista on jaksollisen ilmiön aiheuttamia, vaikka nykyistä kraateriaineistoa laajempi ja tarkempi aineisto olisi tulevaisuudessa saatavilla. Mikäli kaksi kolmasosaa meteoriittitörmäyksistä on jaksollisia, sen havaitseminen on mahdollista, mutta vaatii huomattavasti tämän hetkistä kattavamman kraateriaineiston. Tutkimuksen perusteella on syytä epäillä, että havaittu kraaterien ajallinen jaksollisuus ei ole todellinen ilmiö.

Avainsanat — Nyckelord — Keywords
periodianalyysi, Maan törmäyskraaterit, simulointi

Säilytyspaikka — Förvaringsställe — Where deposited
Tähtitieteen laitos, kirjasto

Muita tietoja — övriga uppgifter — Additional information

Contents

Chapter 1

Introduction

The possible presence of periodicity in the terrestrial impact crater data has been discussed in several papers since 1984. In an article published in the Nature magazine, Alvarez and Muller (1984) detected a 28.4 million year periodicity in the impact cratering on Earth using Fourier analysis. They also found a connection between the periodicity in the impact crater data and the periodicity of 26 million years found by Raup and Sepkoski (1984) in the geological record of the mass extinctions of species.

Davis et al. (1984) and Whitmire and Jackson (1984) offered a distant solar companion as a possible explanation for these periodicities. Davis et al. (1984) suggested that a solar companion in a moderately eccentric orbit could send a large number of comets from the Oort cloud into the inner Solar System when near its closest approach to Sun. Several of these comets would then collide with Earth in the following million years and cause mass extinctions of species, as well as a detectable periodicity in the terrestrial impact crater record. According to Davis et al. (1984) the unseen solar companion would currently be at its maximum distance (about 2.4 light years) from Sun and not pose a threat in another 15 million years. Whitmire and Jackson (1984) proposed independently a similar explanation and concluded that the solar companion's highly eccentric ($e > 0.9$) orbit would have a semi-major axis of about 1.4 light years. They suggested that this companion would be a black dwarf with mass of $0.0002 M_{\odot} < M < 0.07 M_{\odot}$.

An alternative explanation for the periodicity in the impact crater record was offered by Rampino and Stothers (1984) and Schwartz and James (1984). Both papers argued that the interstellar clouds of gas and dust at the galactic plane would gravitationally disturb comets in the Oort cloud and therefore increase the flux of comets to the inner Solar System. Rampino and Stothers (1984) reanalyzed the data used by Raup and Sepkoski (1984) and suggested that the main period in marine life extinctions was 30 ± 1 million years and found this period to closely match the time that the Solar System spends oscillating vertically about

the galactic plane (33±3 million years). They also discovered a similar periodicity of 31 ± 1 million years in the impact crater data on Earth. Recently, the presence of periodicity in the impact crater record has been supported by, among others, Chang and Moon (2005), Chang (2006), Stothers (2006) and Napier (2006).

Trefil and Raup (1987) postulated that the age distribution of craters in the impact crater data could be uniformly periodic, totally random or a combination of the two. Through numerical computation of both real and simulated time series of impact crater events they concluded that the terrestrial impact crater record is created by a mixture of periodic and aperiodic components, so that the random events constitute a majority. Grieve et al. (1988) concluded that it is difficult to consistently detect periodicity in the impact craters record due to aging uncertainties. They analyzed a simulated impact crater data set containing 50% periodic and 50% aperiodic craters and concluded that the correct period could be detected at 99% confidence level only in 50% of the cases where crater aging uncertainties were $< 10\%$ of the periodicity in the data.

The detection of periodicity in the impact crater record has been criticized based on the large uncertainties attached to many impact crater age estimates (e.g. Deutsch and Schaerer, 1994; Grieve and Pesonen, 1996). For example, Grieve and Pesonen (1996) concluded that "Statements regarding a periodicity in the terrestrial cratering record.. are considered unjustified, based on statistical arguments and the large uncertainties attached to many crater age estimates". Similarly, Jetsu (1997) and Jetsu and Pelt (2000) have argued that the detected periods have been due to "human signal": the tendency of rounding uncertain impact crater ages to integer numbers. They found that this rounding enhances spurious periodicities between 10 and 100 million years and apart from these artificial periods, did not find any real periodicity in either impact crater data, nor in the epochs of mass extinctions of species.

The authenticity of the detected periodicity in the terrestrial impact crater data is debatable. It is possible, however, that real periodicity is present and could be detected from more accurate and complete data. In this study we analyze the possibility to detect a real periodicity from the currently available data and, if the current data are found inadequate, we will try to determine the minimum requirements for these data: the quantity (number of craters) and the quality (accuracy in crater ages) that would allow the detection of real periodicity if it were present.

In Chapter 2, we calculate fractional numerical estimates for the detectability of terrestrial impact craters assuming that the impact cratering rate has stayed relatively constant over the time scale covered by this study. The difference in detectability of older and younger craters would therefore be completely due to volcanic and seismic activity, and erosion effects. These fractional estimates

are then utilized in the distribution functions in the following Chapters. In Chapter 3 we define an uncertainty for impact crater ages that is relative to the presumed period in the data. This definition of uncertainty will also be used in the distribution functions in the following Chapters.

Next, we derive the probability density and cumulative distribution functions for crater detectability for the purely periodic (Chapter 5) and aperiodic (Chapter 6) impact cratering cases and for an arbitrary combination of these cases (Chapter 7). Two specific combinations, where the periodic component generates either one or two thirds of all impact craters, are further investigated in the study. Furthermore, we describe the process for creating series of n impact crater ages $t_1, t_2, .., t_n$ from these distribution functions that we use later in our simulations.

The Rayleigh test is introduced and formulated in Chapter 8 as the method used in our period analysis. In Chapter 9, we introduce our simulation hypotheses against which we will later test the statistical significance of our period analysis results. We also compute statistics for these hypotheses H_1, H_2, H_3 and H_4. In Chapter 10, we conduct the main period analysis of our simulated impact crater series of time points and present our results, which are finally discussed in Chapter 11.

Chapter 2

Real data: estimated real detection rate

In this Chapter we derive a model for the detectability of terrestrial impact craters as a function of their age assuming that the terrestrial impact cratering rate has remained constant and the decreasing detectability is completely due to erosion effects.

Neukum and Ivanov (1994) studied the craters on the Moon and arrived at the conclusion that the lunar impact cratering rate has remained constant for about 3000 million years. This would imply that the cratering rate on Earth has also been constant, at least over the past 300 million years covered by this study. If the terrestrial cratering rate has remained constant, the apparent deviation from this steady cratering is solely caused by geological and other processes that reduce the detection rate as a function of crater age. Several geological and other processes influence the detectability of the terrestrial impact craters, e.g. erosion, sedimentary burial, plate tectonics and volcanism. The terrestrial impact cratering rate for the geologically stable areas, such as Australia, North America and Europe, has been investigated by Hughes (2000). He concluded that nearly all craters having a diameter $D > 2.4$ km and an age $t < 125 \pm 20$ My in these regions are still detectable, datable and measurable. The detectability decreases for older craters. For example, in Europe the detectability of craters with $t < 300$ My and $D > 2.4$ km was reduced to 73%.

In this paper, we estimate the detectability of craters by using the same samples already studied in Jetsu (1997) and Jetsu and Pelt (2000). We use two particular sub-samples, where the crater diameter (D), age uncertainty (σ_t) or age (t) have been used as a selection criterion. Similar criteria have been used also in some earlier studies (Grieve and Pesonen, 1996; Matsumoto and Kubotani, 1996) to remove undue bias towards small and young craters which erode away quickly becoming undetectable, and also to eliminate craters whose age is too

uncertain to be useful in period analysis. The selection criteria for these 2nd and 3rd sub-samples of Jetsu (1997) and Jetsu and Pelt (2000) were

$$C_2: \quad \mathrm{t} \leq 250 \text{ My}, \sigma_\mathrm{t} \leq 20 \text{ My}, \quad \mathrm{D} \geq 5 \text{ km} \quad (\mathrm{n} = 34)$$
$$C_3: \quad 5 \text{ My} \leq \mathrm{t} \leq 300 \text{ My}, \quad \sigma_\mathrm{t} \leq 20 \text{ My} \quad (\mathrm{n} = 35).$$

These two crater sub-samples are given in Table 2.1.

We use the data in C_2 and C_3 to provide a direct estimate for the detectability of craters over the whole terrestrial surface based on the above assumption of constant terrestrial cratering rate (Hughes, 2000; Neukum and Ivanov, 1994). We emphasize that our data also contain craters from geologically less stable regions than those studied by Hughes, where the detection probability is lower.

Within C_2 and C_3, these data are divided into ten time intervals of equal length of 25 and 30 My, respectively. That is, we assume ten cycles of equal length during the whole time span of the data in C_2 and C_3. The fraction of craters within each interval is given in the 2nd and 3rd columns of Table 2.2. For example, the first time interval 0 My $\leq$ t $<$ 30 My contains 5 craters out of the total of 35 craters in C_3. Assuming that the cratering rate has remained constant, the detection rate should be monotonically decreasing over time. There are minor fluctuations, which are most probably caused by random effects. For example, the 3rd, 4th and 5th intervals in C_3 gave the fractions 6/35, 2/35 and 6/35. For this reason, we have averaged these fractions of C_2 and C_3 for pairs of consecutive cycles on the 4th and 5th columns of Table 2.2. Both sub-samples contain the same 31 craters, which equals 91% and 89% out of all craters in C_2 and C_3, respectively. Thus the time distributions in both samples are very similar, and we have therefore averaged 4th and 5th columns on the 6th column. These final fractions A_k will be used in our simulations (i.e. as the multipliers A_k in Eqs. 5.3 & 5.4 and 6.3 & 6.5). Hence, the detectability of terrestrial impact craters is introduced into our simulations by multiplying the sum of the periodic and aperiodic distribution functions with these fractions A_k from Table 2.2. In other words, these A_k values are assumed to represent the fractions of craters detected within each particular cycle k, if the cratering rate has remained constant. Note that our definition gives

$$\sum_{k=1}^{K} A_k = 1 \tag{2.1}$$

where $K = 10$ and $k = 1, 2, ...K$.

Table 2.1: Our terrestrial impact crater data: name, location, age ($[t]$ = My), diameter ($[D]$ = km), sub-sample (C_2 or C_3 from Jetsu (1997)), cycle number $k = 1, ...10$ in C_2 or C_3.

Crater	Location	t	D	C_2	C_3	k in C_2	k in C_3
Zhamanshin	Kazakhstan	$\pm.1$	13.5	Yes	No	1	-
Bosumtwi	Ghana	$1.03 \pm .02$	10.5	Yes	No	1	-
El'gygytgyn	Russia	$3.5 \pm .5$	18	Yes	No	1	-
Bigach	Kazakhstan	6 ± 3	7	Yes	Yes	1	1
Shunak	Kazakhstan	12 ± 5	3.1	No	Yes	-	1
Ries/Steinheim	Germany	15 ± 0.7	24.3	Yes	Yes	1	1
Haughton	Canada	23 ± 1	24	Yes	Yes	1	1
Logancha	Russia	25 ± 20	20	Yes	Yes	2	1
Popigai	Russia	35 ± 5	100	Yes	Yes	2	2
Chesapeake Bay	U.S.A	$35.5 \pm .6$	85	Yes	Yes	2	2
Wanapitei	Canada	37 ± 2	7.5	Yes	Yes	2	2
Mistastin	Canada	38 ± 4	28	Yes	Yes	2	2
Logoisk	Belarus	40 ± 5	17	Yes	Yes	2	2
Chiyli	Kazakhstan	46 ± 7	5.5	Yes	Yes	2	2
Kamensk / Gusev	Russia	$49 \pm .14$	25.2	Yes	Yes	2	2
Montagnais	Canada	$50.5 \pm .76$	45	Yes	Yes	3	2
Ragozinka	Russia	55 ± 5	9	Yes	Yes	3	2
Marquez	U.S.A	58 ± 2	13	Yes	Yes	3	2
Chicxulub	Mexico	$64.98 \pm .05$	170	Yes	Yes	3	3
Kara/Ust-Kara	Russia	73 ± 2.1	69.6	Yes	Yes	3	3
Manson	U.S.A	$73.8 \pm .3$	35	Yes	Yes	3	3
Lappajärvi	Finland	$77.3 \pm .4$	23	Yes	Yes	4	3
Boltysh	Ukraine	88 ± 3	24	Yes	Yes	4	3
Dellen	Sweden	89 ± 2.7	19	Yes	Yes	4	3
Steen River	Canada	95 ± 7	25	Yes	Yes	4	4
Carswell/Zapadnava	Canada/Ukraine	115 ± 7.1	39.2	Yes	Yes	5	4
Zeleny Gai	Ukraine	120 ± 20	2.5	No	Yes	-	5
Mien	Sweden	121 ± 2.3	9	Yes	Yes	5	5
Tookoonooka	Australia	128 ± 5	55	Yes	Yes	6	5
Romistrovka	Ukraine	140 ± 20	2.7	No	Yes	-	5
Gosses Bluff	Australia	$142.5 \pm .5$	22	Yes	Yes	6	5
Mjølnir	Norway	143 ± 20	40	Yes	Yes	6	5
Puchenzh-Katunki	Russia	175 ± 3	80	Yes	Yes	8	6
Rochechouart	France	186 ± 8	23	Yes	Yes	8	7
Wells Creek/Red Wing	U.S.A	200 ± 18	15	Yes	Yes	9	7
Manicouagan	Canada	214 ± 1	100	Yes	Yes	9	8
Araguainha Dome	Brazil	247 ± 5.5	40	Yes	Yes	10	9
Clearwater West/East	Canada	290 ± 14	44.4	No	Yes	-	10

Table 2.2: The fraction of the craters within each cycle k: Col. 2 and 3 are the fractions within individual cycles of C_2 and C_3. Col. 4 and 5 are the averaged fractions over two consecutive cycles of C_2 and C_3. The means of Col. 4 and 5 in the last column are the final values for the A_k fractions used in our simulation of artificial crater data.

k	Col. 2	Col. 3	Col. 4	Col. 5	A_k
1	6/34=0.1765	5/35=0.1429	7.0/34=0.2059	7.5/35=0.2143	0.2101
2	8/34=0.2353	10/35=0.2857	7.0/34=0.2059	7.5/35=0.2143	0.2101
3	6/34=0.1765	6/35=0.1714	5.0/34=0.1417	4.0/35=0.1143	0.1307
4	4/34=0.1177	2/35=0.0571	5.0/34=0.1417	4.0/35=0.1143	0.1307
5	2/34=0.0588	6/35=0.1714	2.5/34=0.0735	3.5/35=0.1000	0.0868
6	3/34=0.0882	1/35=0.0286	2.5/34=0.0735	3.5/35=0.1000	0.0868
7	0/34=0.0000	2/35=0.0571	1.0/34=0.0294	1.5/35=0.0429	0.0361
8	2/34=0.0588	1/35=0.0286	1.0/34=0.0294	1.5/35=0.0429	0.0361
9	2/34=0.0588	1/35=0.0286	1.5/34=0.0441	1.0/35=0.0286	0.0363
10	1/34=0.0294	1/35=0.0286	1.5/34=0.0441	1.0/35=0.0286	0.0363

Chapter 3

Real data: average crater age uncertainty

In this Chapter we define a period dependent impact crater age uncertainty that is later used in our simulated data in Chapters 5 and 6.

When compared to geological time scales, impact cratering is an instantaneous event, which in principle allows for precise dating with high resolution. Current impact crater ages have been derived using two fundamentally different approaches: other depend on dating primary shock-related phenomena such as shock metamorphism and displacement of target rocks, others on examining secondary features such as sedimentation and sometimes environmental effects (Deutsch and Schaerer, 1994). Currently only few of the geochronometers used in the impact crater dating provide self-consistent crater ages. It should be noted, that the error estimates given to crater ages in many studies are also often unrealistically small, since the quoted errors only reflect the internal precision of the aging (Deutsch and Schaerer, 1994). In order to establish a comparable definition for dating uncertainties between real impact cratering record and our simulated record (in Chapters 5 and 6), we will define the errors in relation with the proposed periodicity in the data. A similar definition for crater age uncertainty has previously been used e.g. in Grieve et al. (1988).

If we assume K cycles of equal length during the whole time span of the impact crater data $t_1, t_2, .., t_n$, the length of one time interval, i.e. the period P_K will be

$$P_K = \frac{t_n - t_1}{K}. \tag{3.1}$$

Using this period, the aging uncertainty relative to the period P_K for any given crater would be

$$\sigma_P = \frac{\sigma_t}{P_K}, \tag{3.2}$$

where σ_t is the absolute uncertainty of the actual crater age. Finally the average crater age uncertainty for the whole data set would be

$$\bar{\sigma_P} = \frac{1}{n} \sum_{i=1}^{n} \frac{\sigma_{t\,i}}{P_K}, \tag{3.3}$$

where n is the number of craters in the data set and $\sigma_{t\,i}$ is the aging uncertainty for each of the crater ages.

If we use this definition for the actual crater data in Table 2.1 and assume ten ($K = 10$) full cycles of equal length during the whole time span of the data in C_2 and C_3, we will get an average relative uncertainty of $\bar{\sigma_P} = 0.152$ and $\bar{\sigma_P} = 0.186$ for the sub samples C_2 and C_3 respectively as shown in Table 3.1.

Table 3.1: Aging uncertainties for our terrestrial impact crater data. In the last two rows first the average $\bar{\sigma_P}$ of uncertainties σ_P for both sub-samples is calculated and finally the average over these two averages σ_P.

Crater	t	σ_t	P_{K,C_2}	P_{K,C_3}	σ_P for C_2	σ_P for C_3
Zhamanshin	0	0.1	24.7	-	0.004	-
Bosumtwi	1.03	0.02	24.7	-	0.001	-
El'gygytgyn	3.5	0.5	24.7	-	0.020	-
Bigach	6	3	24.7	28.4	0.121	0.106
Shunak	12	5	-	28.4	-	0.176
Ries/Steinheim	15	0.7	24.7	28.4	0.028	0.025
Haughton	23	1	24.7	28.4	0.040	0.035
Logancha	25	20	24.7	28.4	0.810	0.704
Popigai	35	5	24.7	28.4	0.202	0.176
Chesapeake	35.5	0.6	24.7	28.4	0.024	0.021
Wanapitei	37	2	24.7	28.4	0.081	0.070
Mistastin	38	4	24.7	28.4	0.162	0.141
Logoisk	40	5	24.7	28.4	0.202	0.176
Chiyli	46	7	24.7	28.4	0.283	0.246
Kamensk / Gusev	49	0.14	24.7	28.4	0.006	0.005
Montagnais	50.5	0.76	24.7	28.4	0.031	0.027
Ragozinka	55	5	24.7	28.4	0.202	0.176
Marquez	58	2	24.7	28.4	0.081	0.070
Chicxulub	64.98	0.05	24.7	28.4	0.002	0.002
Kara/Ust-Kara	73	2.1	24.7	28.4	0.085	0.074
Manson	73.8	0.3	24.7	28.4	0.012	0.011
Lappajärvi	77.3	0.4	24.7	28.4	0.016	0.014
Boltysh	88	3	24.7	28.4	0.121	0.106
Dellen	89	2.7	24.7	28.4	0.109	0.095
Steen River	95	7	24.7	28.4	0.283	0.246
Carswell/Zapadnava	115	7.1	24.7	28.4	0.287	0.250
Zeleny Gai	120	20	-	28.4	-	0.704
Mien	121	2.3	24.7	28.4	0.093	0.081
Tookoonooka	128	5	24.7	28.4	0.202	0.176
Romistrovka	140	20	-	28.4	-	0.704
Gosses Bluff	142.5	0.5	24.7	28.4	0.020	0.018
Mjølnir	143	20	24.7	28.4	0.810	0.704
Puchenzh-Katunki	175	3	24.7	28.4	0.121	0.106
Rochechouart	186	8	24.7	28.4	0.324	0.282
Wells Creek/Red Wing	200	18	24.7	28.4	0.729	0.634
Manicouagan	214	1	24.7	28.4	0.040	0.035
Araguainha Dome	247	5.5	24.7	28.4	0.223	0.194
Clearwater West/East	290	14	-	28.4	-	0.493
		$\bar{\sigma_P}$ for C_2 and C_4			*0.170*	*0.202*
		Average for $\bar{\sigma_P}$'s			**0.186**	

Chapter 4

Real data: estimated periodicity and aperiodicity

The presence of periodicity in terrestrial impact cratering and mass extinctions of species has been proposed in numerous subsequent studies after the first detections by Alvarez and Muller (1984) and Rampino and Stothers (1984). Even if such periodicity does exist, all impacts on Earth are not necessarily periodic. This has been suggested for example by Trefil and Raup (1987), who conclude that "[crater] record seems to show both periodic and random components, with the random part constituting about two-thirds of the whole". Furthermore, according to Neukum and Ivanov (1994) the cratering rate for the Earth-Moon system has been nearly constant for approximately 3000 million years which indicates that even if a periodic component exists, it may have a relatively low amplitude in comparison with the overall cratering rate. Therefore, when constructing a simulated distribution for the terrestrial impact craters, both periodic and aperiodic impacts must be considered.

Periodic impacts could be due to comets. Periodic "comet showers" from the Oort cloud towards the inner Solar System might be caused by an unseen solar companion "Nemesis" (e.g. Davis et al., 1984; Whitmire and Jackson, 1984) or by the oscillation of Sun in the galactic plane (e.g. Schwartz and James, 1984). If such processes perturb comets into orbits that enter the inner Solar System, the comets will remain in these orbits until they are scattered to new hyperbolic orbits by further perturbations, collide with another body, or are destroyed by close encounters with the Sun. These orbits form a Sun-centered "loss cone" in the comets velocity space. The time that it takes for the comets in this loss cone to be consumed by the aforementioned processes has been studied by Hills (1981). Characteristic survival time for such a comet in orbit with minor axis of $a = 3 \times 10^3$ AU is approximately four orbital periods, or about 7×10^5 yr. On the other hand, the suggested periodicities for the Oort cloud perturbations filling

this loss cone are approximately $2.5-3.0\times10^7$ yr (e.g. Alvarez and Muller, 1984; Rampino and Stothers, 1984; Napier, 2006; Chang, 2006). Thus the time interval between comet showers would be approximately two magnitudes longer than the duration of the shower and for the purposes of this study can be considered to be an "instantaneous" event. The simulation of such a periodic component is formulated in Chapter 5.

Aperiodic impacts are likely to be mostly due to main asteroid belt objects that are transported to Earth crossing orbits by gravitational resonance. For example, numerical simulations have shown that 90% of asteroids injected into 3:1, 5:2 or ν_6 resonances decay in a few million years (Gladman et al., 1997). Since this time scale for the destruction of asteroids on Earth crossing orbits is so short, the simulations predict a much smaller population of Near Earth Asteroids (NEA) than what has been discovered from observations. One possible explanation presented for this problem is a slow "diffusion" of asteroids close to the resonance borders to the actual resonances (Gladman et al., 1997), which has been shown to happen in Kuiper belt (Morbidelli, 1997; Duncan et al., 1995). Gladman et al. (1997) also suggests that a contributing factor to the observed NEA population could be the higher order Jovian resonances (e.g. 8:3 or 9:4) which may induce Earth-crossing asteroid orbits in much longer time scales. Finally, some portion of the NEAs might be old comet nuclei rather than main asteroid belt objects.

It has also been suggested that the terrestrial impacts from the known Earth-crossing meteor streams (especially the Taurid Complex) are not randomly distributed, but may correlate over a time scale of ≈ 10 to 10^4 years (Steel et al., 1994). However, the kinetic energy of these objects would not cause detectable craters, only atmospheric detonations, such as the Tunguska event in 1908. Since these impacts from Earth-crossing meteor streams do not contribute significantly into the impact crater record, this possible periodic mechanism is not considered further in our study. The random temporal distribution of asteroid impacts is further supported by the comparison of simulations against observed fireball data, which shows that the orbital elements of Earth-crossing chondrite asteroids are consistent with steady state injections to 3:1 and ν_6 resonances (Morbidelli and Gladman, 1998). In short, it is relatively safe to assume that the impact events caused by Earth-crossing asteroids can be approximated with an even (i.e. random) distribution, where the impact probability remains constant over time. Our formulation for the aperiodic component simulation is presented in Chapter 6.

The actual ratio between periodic and aperiodic components is unknown. In this paper this ratio will be denoted by S so that a value of $S = 0$ represents a fully periodic case and that of $S = 1$ a fully aperiodic case. This parameter

will be introduced to our simulations in Eqs. 7.1 & 7.2. The formulation for the simulated combination of the aperiodic and periodic cases is given in Chapter 7.

Chapter 5

Simulated data: periodic component

In this Chapter we formulate the simulation of the periodic component of terrestrial impact cratering. We will simulate ten cycles of periodic short impact events. Let the whole time interval be $0 \leq t \leq 10$ and period $P_0 = 1$. Since the duration of each comet shower is assumed to be very much shorter than P_0, the probability density function of these periodic events is approximated with

$$f_1(t) = \delta(t),$$

where $\delta(t)$ is the Dirac delta function. This function is defined by the following relations

$$\begin{aligned} \delta(t - t_0) &= 0, \quad t \neq t_0 \\ \int_{-\infty}^{\infty} \delta(t)dt &= 1 \\ \int_{\infty}^{\infty} g(t)\delta(t - t_0)dt &= g(t_0), \end{aligned}$$

where the $g(t)$ must be a well-behaved function. From this definition it follows that $f_1(t - t_0)$ can be described as an infinitely high thin spike at t_0 (Arfken and Weber, 1995).

Let us assume that the values of A_k represent the fraction of craters detected within the k:th cycle, where $k = 1, 2, ..., K$. The sum of these fractions is $\sum A_k = 1$. The probability distribution function must satisfy $\int_{-\infty}^{\infty} f_1(t)dt = 1$. Hence a suitable form for the respective probability density function is

$$f_P(t) = \sum_{k=1}^{K} A_k f_1(t - t_k),$$

where $t_k = k - \frac{1}{2}$ and $k = 1, 2, ..., K$. Here the subscript P in $f_P(t)$ is adopted to denote the periodic component in the simulated crater distribution. Incidentally, the above definition of $f_P(t)$ is identical to the Dirac comb function

$$\Delta_P(t) = \sum_{k=-\infty}^{\infty} \delta(t - Pk),$$

if $A_k = 1$, $P = P_0 = 1$ and $1 \leq k \leq K$ (Williams, 1999).

Since craters can not be dated with absolute precision, all the crater ages have some uncertainty attached to them. We assume that this uncertainty follows a Gaussian (i.e. *normal*) distribution with a mean μ and a standard deviation σ_P as defined in Chapter 3.

The probability density and cumulative distribution functions are

$$f_G(t, \mu, \sigma_P) = \frac{1}{\sigma\sqrt{2\pi}} \mathrm{e}^{-\frac{1}{2}\left(\frac{t-\mu}{\sigma_P}\right)^2} \tag{5.1}$$

$$F_G(t, \mu, \sigma_P) = \frac{1}{\sigma_P\sqrt{2\pi}} \int_{-\infty}^{t} \mathrm{e}^{-\frac{1}{2}\left(\frac{t'-\mu}{\sigma_P}\right)^2} dt'. \tag{5.2}$$

From the definition of $f_1(t)$ it follows that the convolution with this error distribution $f_G(t, \mu, \sigma_P)$ modifies the probability density functions for the periodic component into the form

$$f_P(t) = \sum_{k=1}^{K} A_k f_G(t - t_k, \mu, \sigma_P).$$

The mean of the error in the ages of the craters is assumed to be $\mu = 0$. Therefore, the following relation

$$f_G(t - t_k, \mu = 0, \sigma_P) = f_G(t, \mu = t_k, \sigma_P) = f_G(t, t_k, \sigma_P)$$

gives the final form of the probability density function

$$f_P(t, \sigma_P) = \sum_{k=1}^{K} A_k f_G(t, t_k, \sigma_P). \tag{5.3}$$

Hence the cumulative distribution function is simply

$$F_P(t, \sigma_P) = \sum_{k=1}^{K} A_k F_G(t, t_k, \sigma_P). \tag{5.4}$$

These two functions $f_P(t, \sigma_P)$ and $F_P(t, \sigma_P)$ are shown in our Fig. 5.1 for the cases $\sigma_P = 0.05, 0.10, 0.20$ and 0.30.

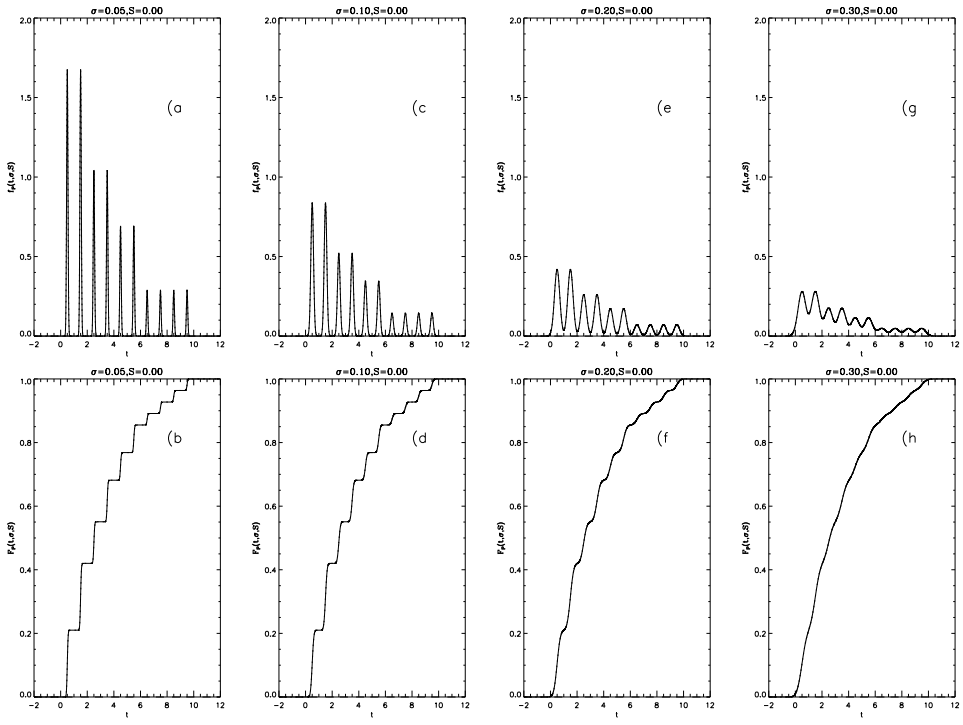

Figure 5.1: Probability density and cumulative distribution functions (Eqs. 5.3 and 5.4) for fully periodic simulated impact events ($S = 0$), where the dating inaccuracies are $\sigma_P = 0.05, 0.10, 0.20$ or 0.30. Note that this case is equivalent to setting $S = 0$ in Eqs. 7.1 & 7.2.

Chapter 6

Simulated data: aperiodic component

In this Chapter we formulate the simulation of the aperiodic component of terrestrial impact cratering. During the cycle k, an aperiodic (i.e. *even* or *random*) component has the following probability density and cumulative distribution functions

$$f_2(t, a_k, b_k) = \begin{cases} 0, & t < a_k \\ \frac{1}{b_k - a_k}, & a_k \leq t \leq b_k \\ 0, & t > b_k, \end{cases}$$

$$F_2(t, a_k, b_k) = \begin{cases} 0, & t < a_k \\ \frac{t - a_k}{b_k - a_k}, & a_k \leq t \leq b_k \\ 1, & t > b_k \end{cases}$$

where $a_k = k - 1$ and $b_k = k$.

Let the values of A_k represent the fraction of craters detected within cycle k, where $k = 1, 2, ..., K$. The sum of these fractions is $\sum A_k = 1$ and the probability distribution function must satisfy $\int_{-\infty}^{\infty} f_2(t)dt = 1$. Hence the forms for the probability density and cumulative distribution functions are

$$f_A(t) = \sum_{k=1}^{K} A_k f_2(t, a_k, b_k) \tag{6.1}$$

$$F_A(t) = \sum_{k=1}^{K} A_k F_2(t, a_k, b_k), \tag{6.2}$$

where the subscript "A" in $f_A(t)$ and $F_A(t)$ is adopted to denote the aperiodic (i.e. random) component in the simulated crater distribution.

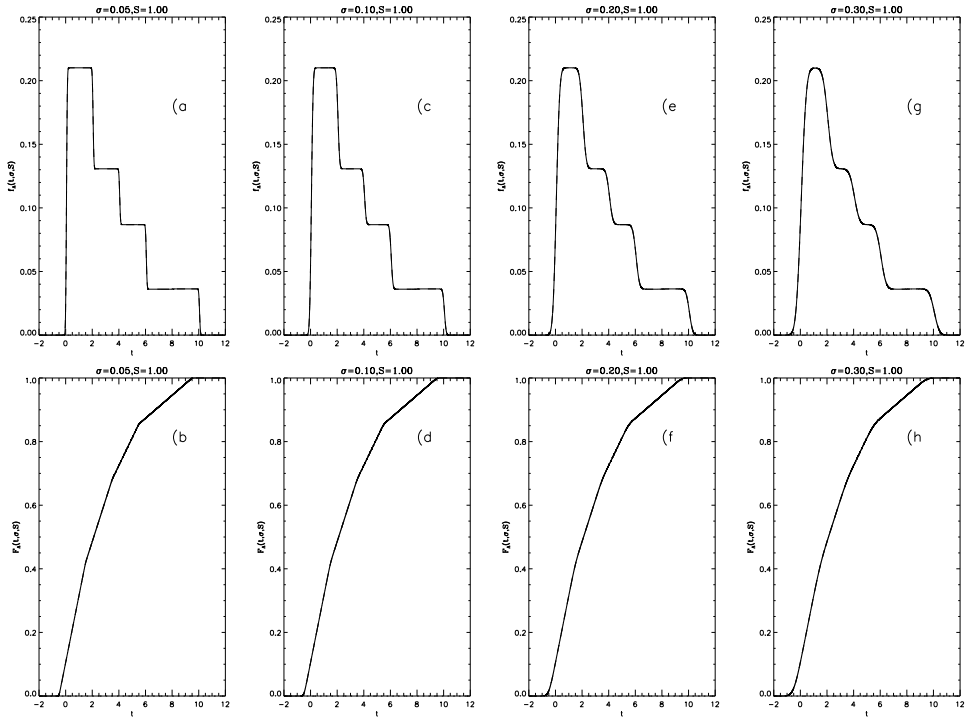

Figure 6.1: Density and cumulative distribution functions (Eqs. 6.3 and 6.5) in the fully aperiodic case, where the dating accuracies are $\sigma_P = 0.05, 0.10, 0.20$ or 0.30. Note again that these are equivalent to the case $S = 1$ in Eqs. 7.1 & 7.2.

Again, an uncertainty is introduced when the ages of the craters are determined. These uncertainties in the ages of the impact craters will modify the above functions $f_A(t)$ and $F_A(t)$. The subsequent forms for these functions are derived in Appendix A.12 (Eqs. A.12 and A.13), where we obtain:

$$f_A(t, \sigma_P) = \sum_{k=1}^{K} A_k \left[F_G(t, k-1, \sigma_P) - F_G(t, k, \sigma_P) \right] \tag{6.3}$$

$$\begin{aligned} F_A(t, \sigma_P) \;\; = \;\; & \sum_{k=1}^{K} A_k \{ \\ & F_G(t, k, \sigma_P) \\ & + (t - k + 1) \left[F_G(t, k-1, \sigma_P) - F_G(t, k, \sigma_P) \right] \\ & + \sigma_P^2 \left[f_G(t, k+1, \sigma_P) - f_G(t, k, \sigma_P) \right] \\ & \}. \end{aligned} \tag{6.4}$$

These functions $f_A(t, \sigma_P)$ and $F_A(t, \sigma_P)$ are shown in our Fig. 6.1 for the cases $\sigma_P = 0.05, 0.10, 0.20$ and 0.30.

Chapter 7

Simulated data: combined components

The probability density function $f_P(t, \sigma_P)$ and the cumulative distribution function $F_P(t, \sigma_P)$ describe the statistics for a fully periodic case (Sect. 5: Eqs. 5.3 and 5.4). The statistics of a fully aperiodic case are described by the respective functions $f_A(t, \sigma_P)$ and $F_A(t, \sigma_P)$ (Sect. 6: Eqs. 6.3 and 6.5). A mixture of these two cases can be described with the functions

$$f_{AP}(t, \sigma_P) = S f_A(t, \sigma_P) + (1 - S) f_P(t, \sigma_P) \quad (7.1)$$

$$F_{AP}(t, \sigma_P) = S F_A(t, \sigma_P) + (1 - S) F_P(t, \sigma_P), \quad (7.2)$$

where the parameter $0 \leq S \leq 1$ determines the relative contribution of the periodic and aperiodic components. The case of $S = 0$ is fully periodic and that of $S = 1$ is fully aperiodic. In this paper, we simulate the cases $S = 0, \frac{1}{3}, \frac{2}{3}$ and 1. The cases $S = 0$ and $S = 1$ have already been displayed in Figs. 5.1 and 6.1. For the two values $S = \frac{1}{3}$ and $\frac{2}{3}$, both components are present simultaneously. These two cases are displayed in Figs. 7.1 and 7.2, respectively.

In this paper we create simulated series of time points of impact crater ages from the cumulative distribution function defined by the Eq. 7.2. A series of n time points is created by first selecting a random sample of $x_1, x_2, .., x_n$ real numbers from an even distribution $[0, 1)$. Then we invert the relation

$$x_k = F_{AP}(t_k, \sigma_P, S), \quad (7.3)$$

which gives the simulated data $t_1, t_2, .., t_n$ for any chosen combination of n, σ_P and S. This idea is depicted in Fig. 7.3.

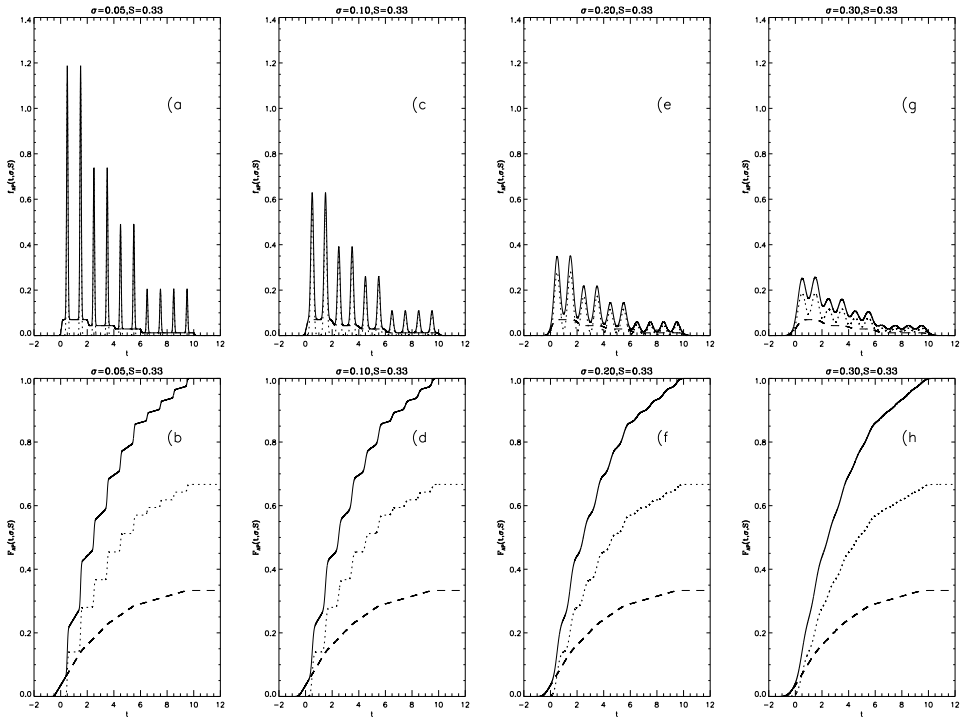

Figure 7.1: The case $S = \frac{1}{3}$ in Eqs. 7.1 & 7.2. The dashed line represents the aperiodic and the dotted line the periodic components, while the continuous line denotes their sum.

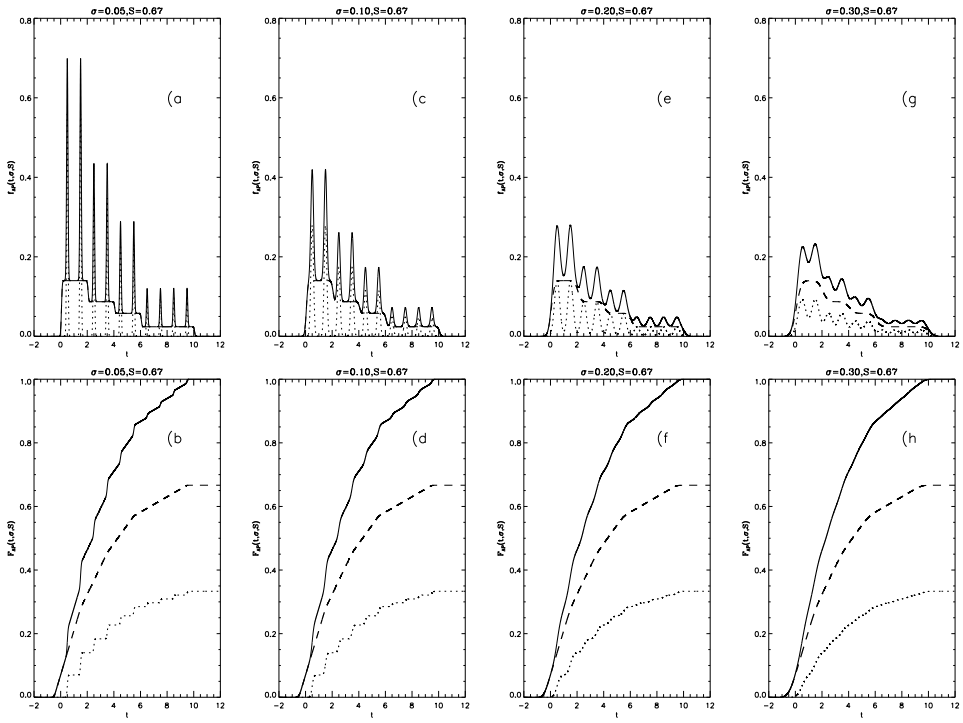

Figure 7.2: The case $S = \frac{2}{3}$ in Eqs. 7.1 & 7.2, otherwise as in Fig. 7.1.

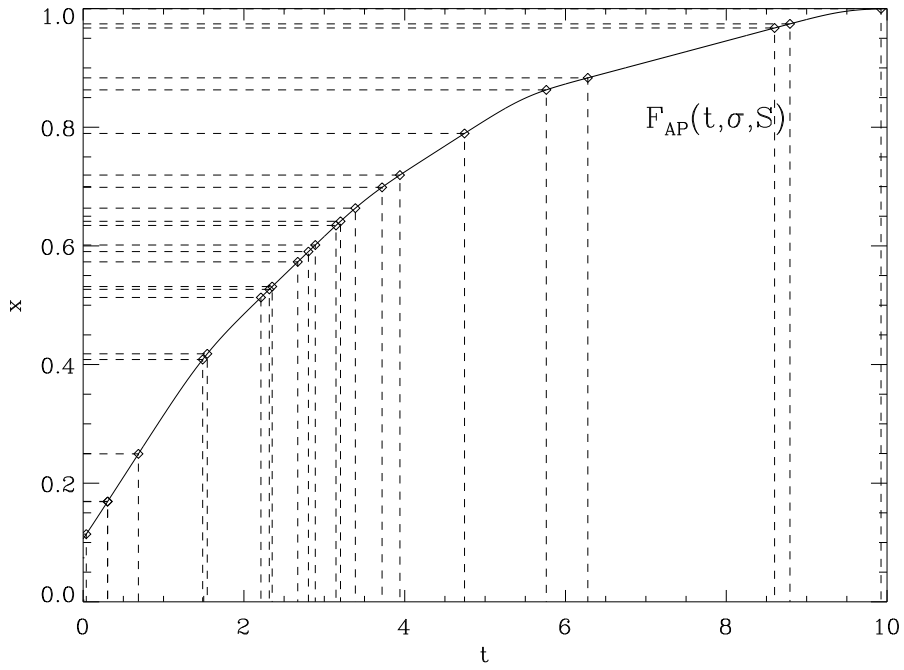

Figure 7.3: The simulated time series of impact craters is derived from cumulative distribution function $F_{AP}(t, \sigma_P, S)$, where $\sigma_P = 0.3$ and $S = 1$. The time series of $t_1 \leq t_2.. \leq t_n$ of $n = 25$ impact crater ages is obtained from the Eq 7.3, where $x_1 \leq x_2.. \leq x_n$ are evenly distributed random numbers between 0 and 1.

Chapter 8

Rayleigh test

In this Chapter we introduce the Rayleigh test and it's statistics. This periodicity test is later used in in our simulations in Chapters 9 and 10.

In astronomy, time points are often sparse and have a low event rate compared to the expected frequency of some periodic phenomena. Individual cycles are not visible in this kind of data, but folding, i.e. splitting the data into parts according to the expected frequency, produces a phase distribution of data. Periodicity can then be detected in this phase distribution using some periodicity test. These *phases* ϕ_i for a series of time points $t_0 \leq t_1 \leq ... \leq t_n$ are calculated with

$$\phi_i = FRAC[(t_i - t_0)P^{-1}] = FRAC[(t_i - t_0)f], \tag{8.1}$$

where $FRAC[x]$ removes the integer part of it's argument x. The relation between period P and frequency f is $f = P^{-1}$. Thus these phases are always $0 \leq \phi_i < 1$.

One of the most widely used non-parametric methods for detecting periodicity is the Rayleigh test (e.g. Kruger et al., 2002). Besides astronomy, Rayleigh test has been used in several other fields, including biology and geology. For example, Batschelet (1981) analyzed the randomness in the observed flight directions of a flight of birds using this method.

Rayleigh method's test statistic or *Rayleigh power* is

$$z = \frac{1}{n}\left[\left(\sum_{i=1}^{n} cos\theta_i\right)^2 + \left(\sum_{i=1}^{n} sin\theta_i\right)^2\right], \tag{8.2}$$

where θ_i is the *phase angle* of phase ϕ_i defined by $\theta_i = 2\pi\phi_i = 2\pi f t_i$. This z measures the directional distribution of the vectors $[cos\theta_i, sin\theta_i]$. It is large when these vectors are pointing to the same direction. Thus the Rayleigh method is sensitive to uni-modal phase distributions. The value for this test statistic z is independent from the chosen zero point t_0 of the time series t_i. In order

to determine the statistics of the Rayleigh power z, we fix the following null hypothesis H_0:

> *"The phases ϕ_i with an arbitrary period P have a random (i.e. even) distribution between $[0, 1)$."*

For this H_0, the density probability function of z for any one arbitrary tested period P is

$$f(z) = e^{-z}. \tag{8.3}$$

By integrating we obtain the cumulative distribution function for z

$$P(z \leq z_0) = F(z_0) = 1 - e^{-z_0}, \tag{8.4}$$

which gives the probability for the test statistic z being equal or less than z_0.

Normally, instead of testing one arbitrary period P, the test is applied to all periods within a certain period range $[P_{min}, P_{max}]$ Since the value for the test statistic z is almost identical for two periods very close to each other, only periods (or frequencies) that are far enough from each other can serve as two independent tests.
The distance (f_0) between two independent tested frequencies is

$$f_0 = \frac{1}{t_n - t_1} = \frac{1}{\Delta T}, \tag{8.5}$$

where $\Delta T = t_n - t_1$. When this small difference f_0 is added to any arbitrary frequency f, the phases of the time points t_n and t_1 are $\Delta T f = x$ and $\Delta T(f + f_0) = x + 1$ (from Eq. 8.1), i.e. the phase difference during the whole time range ΔT is one full cycle. This means that the phases ϕ_i calculated with f and $f + f_0$ are completely rearranged. Therefore, when calculating the periodogram $z(f)$, i.e. the Rayleigh test statistic within the frequency range $[f_{min}, f_{max}]$, we will actually test

$$m = \frac{f_{max} - f_{min}}{f_0} \tag{8.6}$$

independent frequencies. This number m of independent tests has also been empirically verified (Jetsu and Pelt, 1996). Hence, the probability that z reaches z_0 at least once in all these m independent tests is

$$Q = 1 - (1 - e^{-z_0})^m, \tag{8.7}$$

which is hereafter referred as the *critical value* for the Rayleigh test between f_{min} and f_{max}.

The null hypothesis H_0 is rejected if, and only if the critical value Q is less than a preassigned significance level γ. If $Q \leq \gamma$ H_0 is not rejected. The choice

of this preassigned significance level is largely subjective, although in astronomy the values $\gamma = 0.01$ or $\gamma = 0.001$ are often used. Significance level represents the Type I error rate, i.e. it expresses the probability of falsely rejecting H_0 when it is in fact true.

Chapter 9

Simulation of fully aperiodic hypotheses H_1, H_2, H_3 and H_4

The null hypothesis H_0 formulated in Chapter 8 represents a case, where the observed statistical impact crater age distribution is due to random impacts and the detectability of the craters remains constant over time. With these assumptions, there is no reason to suspect that the phases ϕ_i of t_i folded with any arbitrary period P would not be evenly distributed between 0 and 1. However, as discussed in Chapter 2, the detectability of impact craters in the real data decreases as a function of time and therefore H_0 does not necessarily correctly represent the statistical distribution of observed impact crater ages. The statistics of the case where the data are fully aperiodic ($S = 1$), the detectability decreases as a function of time (A_k) and the crater age inaccuracy is σ_P, is hard to derive analytically, but a numerical estimate for it can be determined by computer simulation. We define the following four hypotheses which are used to determine the statistics of our future simulations:

"H_1: The cumulative distribution function is $F_{AP}(t, S = 1, \sigma_P = 0.05)$."

This hypothesis H_1 will be used in the simulations for the cases $F_{AP}(t, S = 0, \sigma_P = 0.05)$, $F_{AP}(t, S = \frac{1}{3}, \sigma_P = 0.05)$ and $F_{AP}(t, S = \frac{2}{3}, \sigma_P = 0.05)$.

"H_2: The cumulative distribution function is $F_{AP}(t, S = 1, \sigma_P = 0.1)$."

This hypothesis H_2 will be used in the simulations for the cases $F_{AP}(t, S = 0, \sigma_P = 0.1)$, $F_{AP}(t, S = \frac{1}{3}, \sigma_P = 0.1)$ and $F_{AP}(t, S = \frac{2}{3}, \sigma_P = 0.1)$.

"H_3: The cumulative distribution function is $F_{AP}(t, S = 1, \sigma_P = 0.2)$."

This hypothesis H_3 will be used in the simulations for the cases $F_{AP}(t, S =$

$0, \sigma_P = 0.2)$, $F_{AP}(t, S = \frac{1}{3}, \sigma_P = 0.2)$ and $F_{AP}(t, S = \frac{2}{3}, \sigma_P = 0.2)$.

"H_4: The cumulative distribution function is $F_{AP}(t, S = 1, \sigma_P = 0.3)$."

This hypothesis H_4 will be used in the simulations for the cases $F_{AP}(t, S = 0, \sigma_P = 0.3)$, $F_{AP}(t, S = \frac{1}{3}, \sigma_P = 0.3)$ and $F_{AP}(t, S = \frac{2}{3}, \sigma_P = 0.3)$.

The statistics for the Rayleigh test with these four hypotheses was calculated by producing a time point series t_i of n impact craters as already described in the end of Chapter 7. The chosen cumulative distribution function in these calculations was that mentioned in each particular hypothesis H_1, H_2, H_3 or H_4.

This simulation of t_i with any particular hypothesis was repeated 100 000 times for each combination of our chosen dating error values $\sigma_P = 0.05, 0.1, 0.2$ & 0.3 and n values $10, 25, 50, 75$ & 100. For each simulated sample $t_1, .., t_n$, the periodogram $z(f)$ was calculated for periodicities between $0.5 \leq P \leq 2.0$ and the highest z value was recorded. In order to prevent the detection of fractions, especially $P = \frac{P_0}{2} = 0.5$, of the period $P_0 = 1$ in our simulations, we disregarded the highest value of z if it was closer than $\frac{f_0}{2}$ to the highest (f_{max}) or the lowest (f_{min}) tested frequency. In other words, only the highest value of $z(f)$ between $f_{min} + \frac{f_0}{2}$ and $f_{max} - \frac{f_0}{2}$ was recorded. By sorting these 100 000 highest z values for each combination of n and σ_P in to ascending order we created a numerical estimate for the minimum value z_0 that corresponds to the chosen preassigned significance level γ. In this study, we have chosen to test the data against the critical levels $\gamma = 0.01$ and $\gamma = 0.001$. The corresponding numerical estimates for z_0 are presented in Table 9.1.

The values in Table 9.1 will be used in the next Chapter to determine the statistical significance of found periodicities. For example, the hypothesis H_1 gives the probability that $P(z \geq z_0) = 0.01$ when $z_0 = 6.861$ for $n = 10$ and $\sigma_P = 0.05$. This particular limit will be used for $n = 10$ in cases, where the simulated distribution is $F_{AP}(t, S = 0, \sigma_P = 0.05)$, $F_{AP}(t, S = \frac{1}{3}, \sigma_P = 0.05)$ or $F_{AP}(t, S = \frac{2}{3}, \sigma_P = 0.05)$

Table 9.1: Numerical simulated estimates of the z_0 limit for Rayleigh test statistic z that correspond to the critical values $Q = 0.01$ and $Q = 0.001$ under the hypothesis H_1, H_2, H_3 or H_4.

	H_1		H_2	
n	$P(z \geq z_0) = 0.01$	$P(z \geq z_0) = 0.001$	$P(z \geq z_0) = 0.01$	$P(z \geq z_0) = 0.001$
10	$z_0 = 6.861$	$z_0 = 8.060$	$z_0 = 6.902$	$z_0 = 8.149$
25	$z_0 = 7.907$	$z_0 = 9.975$	$z_0 = 7.885$	$z_0 = 9.838$
50	$z_0 = 8.427$	$z_0 = 10.708$	$z_0 = 8.284$	$z_0 = 10.667$
75	$z_0 = 8.728$	$z_0 = 11.375$	$z_0 = 8.608$	$z_0 = 11.155$
100	$z_0 = 9.073$	$z_0 = 11.719$	$z_0 = 8.878$	$z_0 = 11.534$
	H_3		H_4	
n	$P(z \geq z_0) = 0.01$	$P(z \geq z_0) = 0.001$	$P(z \geq z_0) = 0.01$	$P(z \geq z_0) = 0.001$
10	$z_0 = 6.884$	$z_0 = 8.188$	$z_0 = 6.803$	$z_0 = 8.077$
25	$z_0 = 7.735$	$z_0 = 9.912$	$z_0 = 7.687$	$z_0 = 9.703$
50	$z_0 = 8.070$	$z_0 = 10.367$	$z_0 = 7.995$	$z_0 = 10.324$
75	$z_0 = 8.283$	$z_0 = 10.587$	$z_0 = 8.114$	$z_0 = 10.475$
100	$z_0 = 8.495$	$z_0 = 11.018$	$z_0 = 8.213$	$z_0 = 10.764$

Chapter 10

Simulation of different cases of periodicity

In this Chapter, we determine the probability of finding the correct period $P_0 = 1$ with the Rayleigh test from the time point series derived out of our chosen simulated cumulative distribution function. The impact crater data of n crater ages t_i were created from the cumulative distribution function (Eq. 7.2) using the same procedure as described in Chapter 9.

We performed 100 000 simulations for each combination of n, σ_P and S. In each simulation, the periodogram $z(f)$ was calculated for the frequency range $0.5 \leq f \leq 2.0$. We selected the highest value for z from this range and recorded the corresponding period P. Again, as in Chapter 9, in order to prevent the detection of fractions, especially $P = \frac{P_0}{2} = 0.5$, of the correct period $P_0 = 1$ in our simulated distribution F_{AP} we accepted only the highest value of $z(f)$ between $f_{min} + \frac{f_0}{2}$ and $f_{max} - \frac{f_0}{2}$. The statistical significance of this detected best period was compared to our numerical estimates z_0 for corresponding simulation hypothesis H_1, H_2, H_3 or H_4. The values for these z_0 were taken from the Table 9.1. The equivalent significance was also computed from the the analytical estimate (Eq. 8.7) for null hypothesis H_0. Furthermore, we derived the result for two significance levels: $\gamma = 0.01$ and $\gamma = 0.001$.

If the detected period P was statistically significant, we examined if this period was the same as the correct period $P_0 = 1$ embedded in our simulations. We accepted the detected period P as correct if its corresponding frequency $f = \frac{1}{P}$ fell within $\frac{1}{P_0} - \frac{f_0}{2} \geq f \geq \frac{1}{P_0} + \frac{f_0}{2}$, where f_0 is the distance between the independent frequencies (Eq. 8.5). Periods P outside this range were considered incorrect. Finally, statistically significant periods, both correct and incorrect ones separately, were counted and divided by the number of simulations (i.e. 100 000) in order to get the probabilities for detecting the period for each of these cases. All results of the simulations are presented in Tables 10.1 – 10.6.

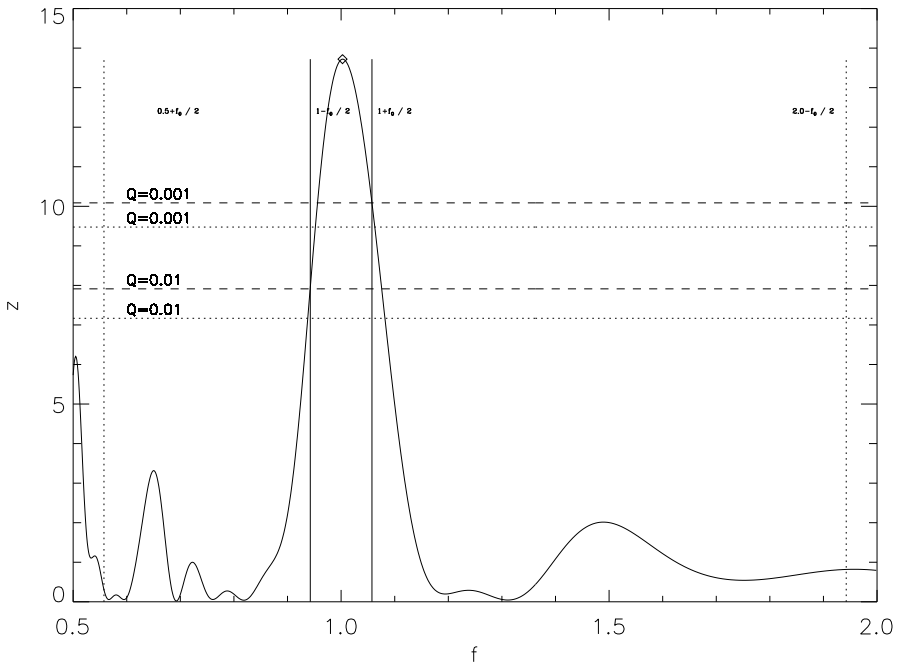

Figure 10.1: Example of a periodogram calculated from simulated data with $S = \frac{1}{3}$, $n = 25$ and $\sigma_P = 0.1$. The limits for z_0 having $\gamma = 0.01$ and 0.001 are shown in dotted line for H_0 (from Eq. 8.4, $z_0 = -ln[1-(1-Q)^{\frac{1}{m}}]$) and the dashed line for H_1 (from Table 9.1). The highest z exceeds the levels $Q \leq \gamma = 0.01$ and $Q \leq \gamma = 0.001$ for both H_0 and H_1. The corresponding best detected frequency f satisfies the criterion $\frac{1}{P_0} - \frac{f_0}{2} \geq f \geq \frac{1}{P_0} + \frac{f_0}{2}$, which is limited by the two solid vertical lines. The two dashed vertical lines represent the limits for $f_{min} + \frac{f_0}{2}$ and $f_{max} - \frac{f_0}{2}$.

Table 10.1: Results of simulations for $F_{AP}(t, S = 0, \sigma_P = 0.05)$, $F_{AP}(t, S = 0, \sigma_P = 0.1)$, $F_{AP}(t, S = 0, \sigma_P = 0.2)$ and $F_{AP}(t, S = 0, \sigma_P = 0.3)$ tested against hypotheses H_0, H_1, H_2, H_3 and H_4 with significance level $\gamma = 0.01$. Cases where the correct period was found in 95 % or more of all 100 000 simulations are marked in bold. Cases where periodicity was not found in any of the 100 000 simulation rounds are marked with an integer zero.

	$\gamma = 0.01$		$\gamma = 0.01$	
	correct $\lvert 1 - f \rvert \leq \frac{f_0}{2}$	incorrect $\lvert 1 - f \rvert > \frac{f_0}{2}$	correct $\lvert 1 - f \rvert \leq \frac{f_0}{2}$	incorrect $\lvert 1 - f \rvert > \frac{f_0}{2}$
	H_1		H_0	
10	**0.999**	0.001	**0.999**	0.001
25	**1.000**	0	**1.000**	0
50	**1.000**	0	**1.000**	0
75	**1.000**	0	**1.000**	0
100	**1.000**	0	**1.000**	0
	H_2		H_0	
10	0.676	0.012	0.685	0.011
25	**1.000**	0.000	**1.000**	0.000
50	**1.000**	0	**1.000**	0
75	**1.000**	0	**1.000**	0
100	**1.000**	0	**1.000**	0
	H_3		H_0	
10	0.031	0.013	0.035	0.013
25	0.298	0.019	0.379	0.030
50	0.831	0.012	0.888	0.017
75	**0.979**	0.004	**0.989**	0.004
100	**0.998**	0.001	**0.999**	0.001
	H_4		H_0	
10	0.003	0.011	0.003	0.010
25	0.008	0.012	0.013	0.023
50	0.023	0.018	0.039	0.036
75	0.050	0.024	0.081	0.047
100	0.087	0.029	0.136	0.058

Table 10.2: As Table 10.1 but with $\gamma = 0.001$.

	$\gamma = 0.001$		$\gamma = 0.001$	
	correct $\lvert 1-f\rvert \leq \frac{f_0}{2}$	incorrect $\lvert 1-f\rvert > \frac{f_0}{2}$	correct $\lvert 1-f\rvert \leq \frac{f_0}{2}$	incorrect $\lvert 1-f\rvert > \frac{f_0}{2}$
	H_1		H_0	
10	**0.993**	0.001	0.597	0.001
25	**1.000**	0	**1.000**	0
50	**1.000**	0	**1.000**	0
75	**1.000**	0	**1.000**	0
100	**1.000**	0	**1.000**	0
	H_2		H_0	
10	0.259	0.004	0.040	0.001
25	**1.000**	0.000	**1.000**	0.000
50	**1.000**	0	**1.000**	0
75	**1.000**	0	**1.000**	0
100	**1.000**	0	**1.000**	0
	H_3		H_0	
10	0.004	0.001	0.000	0.000
25	0.106	0.003	0.140	0.005
50	0.620	0.005	0.712	0.007
75	0.927	0.002	**0.959**	0.003
100	**0.991**	0.000	**0.997**	0.001
	H_4		H_0	
10	0.000	0.001	0.000	0.000
25	0.001	0.001	0.001	0.002
50	0.004	0.002	0.008	0.005
75	0.012	0.004	0.023	0.007
100	0.024	0.005	0.046	0.011

Table 10.3: Results of simulations for $F_{AP}(t, S = \frac{1}{3}, \sigma_P = 0.05)$, $F_{AP}(t, S = \frac{1}{3}, \sigma_P = 0.1)$, $F_{AP}(t, S = \frac{1}{3}, \sigma_P = 0.2)$ and $F_{AP}(t, S = \frac{1}{3}, \sigma_P = 0.3)$ tested against hypotheses H_0, H_1, H_2, H_3 and H_4, with significance level $\gamma = 0.01$. Cases where the probability of finding an incorrect period is higher than that of finding the correct one are in italics. Otherwise as in Table 10.1.

	$\gamma = 0.01$		$\gamma = 0.01$	
	correct $\lvert 1 - f \rvert \leq \frac{f_0}{2}$	incorrect $\lvert 1 - f \rvert > \frac{f_0}{2}$	correct $\lvert 1 - f \rvert \leq \frac{f_0}{2}$	incorrect $\lvert 1 - f \rvert > \frac{f_0}{2}$
	H_1		H_0	
10	0.205	0.003	0.208	0.014
25	0.777	0.003	0.837	0.012
50	**0.995**	0.000	**0.998**	0.001
75	**1.000**	0.000	**1.000**	0.000
100	**1.000**	0	**1.000**	0
	H_2		H_0	
10	0.099	0.013	0.104	0.013
25	0.560	0.012	0.651	0.019
50	**0.962**	0.002	**0.980**	0.003
75	**0.998**	0.000	**0.999**	0.000
100	**1.000**	0	**1.000**	0
	H_3		H_0	
10	*0.009*	*0.010*	0.010	0.009
25	0.052	0.013	0.077	0.024
50	0.226	0.018	0.308	0.032
75	0.457	0.018	0.571	0.032
100	0.669	0.014	0.778	0.023
	H_4		H_0	
10	*0.002*	*0.010*	*0.002*	*0.008*
25	*0.003*	*0.010*	*0.005*	*0.019*
50	*0.006*	*0.011*	*0.011*	*0.025*
75	*0.011*	*0.013*	*0.020*	*0.029*
100	0.017	0.014	*0.031*	*0.032*

Table 10.4: As Table 10.3 but with $\gamma = 0.001$.

	$\gamma = 0.001$		$\gamma = 0.001$	
	correct $\lvert 1-f\rvert \leq \frac{f_0}{2}$	incorrect $\lvert 1-f\rvert > \frac{f_0}{2}$	correct $\lvert 1-f\rvert \leq \frac{f_0}{2}$	incorrect $\lvert 1-f\rvert > \frac{f_0}{2}$
	H_1		H_0	
10	0.107	0.003	0.034	0.000
25	0.587	0.003	0.643	0.004
50	**0.979**	0.000	**0.989**	0.000
75	**1.000**	0.000	**1.000**	0.000
100	**1.000**	0	**1.000**	0
	H_2		H_0	
10	0.026	0.002	0.004	0.000
25	0.335	0.003	0.382	0.004
50	0.882	0.001	0.929	0.002
75	**0.992**	0.000	**0.997**	0.000
100	**1.000**	0	**1.000**	0
	H_3		H_0	
10	0.001	0.001	*0.000*	*0.000*
25	0.011	0.001	0.016	0.003
50	0.084	0.003	0.126	0.006
75	0.241	0.005	0.330	0.009
100	0.424	0.004	0.565	0.008
	H_4		H_0	
10	*0.000*	*0.001*	*0*	*0.000*
25	*0.000*	*0.001*	*0.001*	*0.002*
50	*0.001*	*0.001*	*0.002*	*0.003*
75	0.002	0.001	0.004	0.004
100	0.003	0.001	0.007	0.004

Table 10.5: Results of simulations for $F_{AP}(t, S = \frac{2}{3}, \sigma_P = 0.05)$, $F_{AP}(t, S = \frac{2}{3}, \sigma_P = 0.1)$, $F_{AP}(t, S = \frac{2}{3}, \sigma_P = 0.2)$ and $F_{AP}(t, S = \frac{2}{3}, \sigma_P = 0.3)$ tested against hypotheses H_0, H_1, H_2, H_3 and H_4,with significance level $\gamma = 0.01$. Otherwise as in Table 10.3.

	$\gamma = 0.01$		$\gamma = 0.01$	
	correct $\lvert 1 - f \rvert \leq \frac{f_0}{2}$	incorrect $\lvert 1 - f \rvert > \frac{f_0}{2}$	correct $\lvert 1 - f \rvert \leq \frac{f_0}{2}$	incorrect $\lvert 1 - f \rvert > \frac{f_0}{2}$
	H_1		H_0	
10	0.015	0.012	0.016	0.011
25	0.070	0.013	0.107	0.027
50	0.248	0.014	0.356	0.034
75	0.476	0.013	0.620	0.031
100	0.666	0.010	0.803	0.023
	H_2		H_0	
10	*0.008*	*0.009*	*0.009*	*0.009*
25	0.037	0.012	0.060	0.024
50	0.142	0.015	0.217	0.033
75	0.296	0.014	0.428	0.034
100	0.459	0.012	0.621	0.030
	H_3		H_0	
10	*0.002*	*0.008*	*0.002*	*0.008*
25	*0.005*	*0.010*	*0.009*	*0.019*
50	0.014	0.011	0.025	0.024
75	0.028	0.011	0.052	0.028
100	0.045	0.011	0.086	0.032
	H_4		H_0	
10	*0.001*	*0.010*	*0.001*	*0.008*
25	*0.001*	*0.009*	*0.002*	*0.016*
50	*0.002*	*0.009*	*0.003*	*0.020*
75	*0.002*	*0.094*	*0.004*	*0.021*
100	*0.003*	*0.009*	*0.005*	*0.022*

Table 10.6: As Table 10.5 but with $\gamma = 0.001$.

	$\gamma = 0.001$		$\gamma = 0.001$	
	correct $\lvert 1-f\rvert \leq \frac{f_0}{2}$	incorrect $\lvert 1-f\rvert > \frac{f_0}{2}$	correct $\lvert 1-f\rvert \leq \frac{f_0}{2}$	incorrect $\lvert 1-f\rvert > \frac{f_0}{2}$
	H_1		H_0	
10	0.004	0.002	0.001	0.000
25	0.021	0.002	0.030	0.003
50	0.112	0.003	0.176	0.007
75	0.258	0.003	0.404	0.009
100	0.444	0.003	0.629	0.008
	H_2		H_0	
10	0.001	0.001	0.000	0.000
25	0.009	0.002	0.013	0.003
50	0.047	0.002	0.083	0.006
75	0.127	0.002	0.224	0.008
100	0.240	0.002	0.399	0.008
	H_3		H_0	
10	*0.000*	*0.001*	*0.000*	*0.000*
25	*0.001*	*0.001*	*0.001*	*0.001*
50	0.002	0.001	0.005	0.003
75	0.006	0.001	0.012	0.004
100	0.011	0.001	0.025	0.005
	H_4		H_0	
10	*0.000*	*0.001*	*0*	*0.000*
25	*0.000*	*0.001*	*0.000*	*0.001*
50	*0.000*	*0.001*	*0.000*	*0.002*
75	*0.000*	*0.001*	*0.001*	*0.002*
100	*0.000*	*0.001*	*0.001*	*0.002*

Chapter 11

Discussion and Conclusions

In this Chapter we discuss our results, which are summarized in Tables 11.1 and 11.2. We also compare our results to those of Grieve et al. (1988) and comment on the detection of a period of 28.4 million years by Alvarez and Muller (1984) in the light of our simulations. Finally, we argue whether it is achievable to reliably detect a possible real periodicity in the most recent impact crater data.

We raised a set of questions in the first Chapter relating to the quantity and quality (i.e. the dating accuracy) of impact crater time points that would allow detection of real periodicity in the cratering record. In order to answer these questions we postulate that detecting the periodicity is "certain" when we have found the correct period P_0 with the chosen preassigned significance level in more than 95 % of the simulation rounds. These cases had a value of ≥ 0.950 in our Tables 10.1 – 10.6.

The choice of the hypothesis that the simulated crater data was tested against, either the null hypothesis H_0 or one of H_1, H_2, H_3 or H_4, had little effect on the results. In only two cases ($n = 10$, $S = 0$ & $\sigma_P = 0.05$ and $n = 75$, $S = 0$ & $\sigma_P = 0.2$, both connected to the preassigned significance level $\gamma = 0.001$), was the correct periodicity detected with certainty with our hypothesis (in this case H_1 and H_3), while the same periodicity was not detected with the null hypothesis H_0. In general, with significance level of $\gamma = 0.001$ the hypothesis H_1, H_2, H_3 or H_4 had a slightly higher chance of finding the correct period than H_0, while with significance level of $\gamma = 0.01$ the result was the opposite. One contributing factor to this behaviour is that with small n ($n < 50$) the assumption of asymptotic density distribution (Eq. 8.3) of the Rayleigh power z does not hold (Brazier, 1994). Since the results obtained when applying the different hypotheses do not differ significantly, we will limit the following analysis only to the cases H_1, H_2, H_3 and H_4, which we believe to give a more reliable representation for the real crater data.

Using the above definition for "certain" detection, when $S = 0$, that is all the

Table 11.1: The minimum number n of simulated impact crater time points t_i needed to detect the correct periodicity at the preassigned significance level of $\gamma = 0.01$ when tested against hypotheses H_1, H_2, H_3 or H_4. The cases where periodicity could not be detected with certainty for $n \leq 100$ are denoted with "never".

	H_1 $\sigma_P = 0.05$	H_2 $\sigma_P = 0.1$	H_3 $\sigma_P = 0.2$	H_4 $\sigma_P = 0.3$
$S = 0$	$n \geq 10$	$n \geq 25$	$n \geq 75$	never
$S = \frac{1}{3}$	$n \geq 50$	$n \geq 50$	never	never
$S = \frac{2}{3}$	never	never	never	never

Table 11.2: The minimum number n of simulated impact crater time points t_i needed to detect the correct periodicity at the preassigned significance level $\gamma = 0.001$. Otherwise as in Table 11.1.

	H_1 $\sigma_P = 0.05$	H_2 $\sigma_P = 0.1$	H_3 $\sigma_P = 0.2$	H_4 $\sigma_P = 0.3$
$S = 0$	$n \geq 10$	$n \geq 25$	$n \geq 100$	never
$S = \frac{1}{3}$	$n \geq 50$	$n \geq 75$	never	never
$S = \frac{2}{3}$	never	never	never	never

impact events are caused by periodic phenomena, the dating uncertainties of the craters can not exceed $\sigma_P = 0.2$, if the periodicity is to be detected in the data with the tested number of values t_i below $n = 100$. For $\sigma_P = 0.2$, the period is reliably found with $n \geq 75$ when $\gamma = 0.01$ and with $n \geq 100$ when $\gamma = 0.001$. When one third of the cratering is caused by random events ($S = \frac{1}{3}$), $P_0 = 1$ was reliably found only when crater age uncertainties are $\sigma_P \leq 0.1$. For the statistical significance $\gamma = 0.01$, the required number of crater events was $n \geq 50$ while for $\gamma = 0.001$ it was $n \geq 75$. When two thirds of the impact craters were aperiodic ($S = \frac{2}{3}$), we were unable to find the periodicity with certainty in any of our simulated cases. The probability of finding the correct period did not rise above 66.6 % for any of the tested cases of n and σ_P.

In many cases where the correct periodicity could not be found in 95 % of all simulations, there was also a slight chance of finding an incorrect period. For example, when $S = \frac{1}{3}$, $\sigma_P = 0.1$, $\gamma = 0.01$ and $n = 25$, there was a 56 % probability of finding the correct period, but also a 1.2 % probability of finding an incorrect one (Table 10.3, hypothesis H_2, row two). When $S = \frac{1}{3}$ or $S = \frac{2}{3}$ and $\sigma_P = 0.3$, detecting an incorrect period was more likely than detecting a correct one for majority of the tested n. This phenomenon was more prominent with $\gamma = 0.01$ than with $\gamma = 0.001$ as could be expected, since lowering the significance level reduces the probability of falsely rejecting the null hypothesis, i.e. finding periodicity in data where it is in reality not present.

The impact crater event data used in Alvarez and Muller (1984) is presented in Table 11.3. The mean error of this data is $\bar{\sigma_P} = 0.240 \approx 0.2$ and since two of the craters (Logoisk and Boltysh) have the same age this is equivalent to the case $n = 10$. Our data shows that if all these craters were due to periodic impacts, the probability for detecting (with statistical significance of $\gamma = 0.01$) a real periodicity in this data is 3 %. If one third of these impacts were aperiodic ($S = \frac{1}{3}$) respective probability falls to 0.9 % and with two thirds of aperiodic events ($S = \frac{2}{3}$) gives only 0.2 %. It seems therefore highly unlikely that the periodicity detected by Alvarez & Muller would be a real signal caused by periodic impact cratering events. A more probable explanation for this finding could be some spurious periodicity caused by, for example, the crater age rounding effect proposed in Jetsu (1997) and Jetsu and Pelt (2000).

The fractions A_k were derived from the sample of impact craters used in the earlier papers (Jetsu, 1997; Jetsu and Pelt, 2000). We are aware that since then the impact crater data has improved in both number of t_i values and dating accuracy σ_t. In Appendix B, we study a more recent set of impact crater data using the impact crater catalogue of *The Earth Impact Database* maintained by the Planetary and Space Science Centre at the University of New Brunswick. Two sub-samples were taken from these more recent data that fulfilled the cri-

Table 11.3: Impact crater data from which Alvarez and Muller (1984) detected the period $P = 28.4$. This periodicity was used to calculate the relative uncertainties σ_P. The ages (t) and uncertainties (σ_t, σ_p) are presented in millions of years and crater diameters (D) in kilometers.

Crater	Location	D	t	σ_t	σ_P
Karla	Russia	10	7	4	0.317
Ries/Steinheim	Germany	24	14.8	0.7	0.141
Mistastin	Canada	28	38	4	0.246
Popigai	Russia	100	39	9	0.704
Lappajärvi	Finland	14	77	4	0.176
Steen River	Canada	25	95	7	0.211
Logoisk	Belarus	17	100	20	0.176
Boltysh	Ukraine	25	100	5	0.141
Gosses Bluff	Australia	22	130	6	0.211
Rochechouart	France	23	160	5	0.176
Manicouagan	Canada	70	210	4	0.141
Average error $\bar{\sigma_P}$ of the data					*0.240*

terion C_2 or C_3 from Jetsu (1997) is presented in the Table B.1. The larger sub-sample C_3 has $n = 45 \approx 50$ records and $\sigma_P = 0.193 \approx 0.2$. According to our simulations, the probability of finding the real period in these C_3 data with $S = 0$ is 83 % ($\gamma = 0.01$) or 62 % ($\gamma = 0.001$). With $S = \frac{1}{3}$ the respective probabilities are ≈ 22 % ($\gamma = 0.01$) or ≈ 8 % ($\gamma = 0.001$). Finally, with $S = \frac{2}{3}$ the respective probabilities fall to ≈ 1 % ($\gamma = 0.01$) and 0.2 % ($\gamma = 0.001$). In other words, current impact crater data are not sufficient to confidently detect a possible real periodic signal. This is mainly due to the large uncertainties in the crater age data. It should also be considered, that even these large uncertainties might be underestimated (Deutsch and Schaerer, 1994). Our results more or less confirm the conclusion of Grieve et al. (1988):

> "It is difficult to consistently detect a period from a mixture of periodic and random ages, unless the record is either dominated by the periodic ages or the ages have small uncertainties (< 10 %) in respect to the period in question".

Currently the quantitative value of the ratio between periodic and aperiodic events is not known, although the apparently constant terrestrial cratering rate over the last 3000 million years (Neukum and Ivanov, 1994), the observed number of Near Earth Asteroids, the behavior of asteroid belt objects at Jovian resonances (Gladman et al., 1997) and the results in Trefil and Raup (1987) could

indicate that a major portion of the impact craters are caused by aperiodic events. If this is the case, according to our simulations the detection of real periodicity is very difficult even though the crater ages in the data would have smaller uncertainties in the future. If the random component dominates, the detection of real periodicity might only be possible with several hundred highly accurate terrestrial impact crater ages. Considering that the number of craters in the C_3 sub-sample has increased only by ten and C_2 sub-sample by four in the last decade, this is not likely to happen in the near future. Thus, the question of periodicity in the terrestrial impact crater record might remain without final answer for the foreseeable future.

11.1 Acknowledgements

First of all I would like to thank my tutor docent Lauri Jetsu and vice-tutors M.S. Sebastian Porceddu and M.S. Perttu Kajatkari for their valuable comments and suggestions without which this work would not have become what it is. Working with them has been an inspiration and a pleasure.

I would like also to show gratitude to my parents whose subtle and sometimes not so subtle encouragement contributed to me finally finishing this work. Lastly, above all I would like to thank my wife Ilana for her support and patience and my son Eelis.

References

W. Alvarez and R. A. Muller. Evidence from crater ages for periodic impacts on the earth. Nature, 308:718–720, April 1984. 1, 11, 12, 36, 38, 39

G. B. Arfken and H. J. Weber. *Mathematical Methods for Physicists*, volume Fourth. Academic Press, 1995. 14

E Batschelet. *Circular statistics in biology*. Academic Press, London, 1981. 22

K. T. S. Brazier. Confidence Intervals from the Rayleigh Test. MNRAS, 268: 709–+, June 1994. 36

H.-Y. Chang. Time/Frequency Analysis of Terrestrial Impack Crater Records. *Journal of Astronomy and Space Sciences*, 23:199–208, September 2006. 2, 12

H.-Y. Chang and H.-K. Moon. Time-Series Analysis of Terrestrial Impact Crater Records. PASJ, 57:487–495, June 2005. 2

M. Davis, P. Hut, and R. A. Muller. Extinction of species by periodic comet showers. Nature, 308:715–717, April 1984. 1, 11

A. Deutsch and U. Schaerer. Dating terrestrial impact events. *Meteoritics*, 29: 301–322, May 1994. 2, 8, 39, 50

M. J. Duncan, H. F. Levison, and S. M. Budd. The Dynamical Structure of the Kuiper Belt. AJ, 110:3073–+, December 1995. 12

B. J. Gladman, F. Migliorini, A. Morbidelli, V. Zappala, P. Michel, A. Cellino, C. Froeschle, H. F. Levison, M. Bailey, and M. Duncan. Dynamical lifetimes of objects injected into asteroid belt resonances. *Science*, 277:197–201, 1997. 12, 39

R. A. F. Grieve and L. J. Pesonen. Terrestrial Impact Craters: Their Spatial and Temporal Distribution and Impacting Bodies. *Earth Moon and Planets*, 72:357–376, February 1996. 2, 4

R. A. F. Grieve, V. L. Sharpton, J. D. Rupert, and A. K. Goodacre. Detecting a periodic signal in the terrestrial cratering record. In G. Ryder, editor, *Lunar and Planetary Science Conference*, volume 18 of *Lunar and Planetary Science Conference*, pages 375–382, 1988. 2, 8, 36, 39

J. G. Hills. Comet showers and the steady-state infall of comets from the Oort cloud. AJ, 86:1730–1740, November 1981. 11

D. W. Hughes. A new approach to the calculation of the cratering rate of the Earth over the last 125+/-20Myr. MNRAS, 317:429–437, September 2000. 4, 5

L. Jetsu. The "human" statistics of terrestrial impact cratering rate. A&A, 321: L33–L36, May 1997. 2, 4, 5, 6, 38, 39, 49, 51

L. Jetsu and J. Pelt. Searching for periodicity in weighted time point series. A&AS, 118:587–594, September 1996. 23

L. Jetsu and J. Pelt. Spurious periods in the terrestrial impact crater record. A&A, 353:409–418, January 2000. 2, 4, 5, 38, 49

A. T. Kruger, T. J. Loredo, and I. Wasserman. Search for High-Frequency Periodicities in Time-tagged Event Data from Gamma-Ray Bursts and Soft Gamma Repeaters. ApJ, 576:932–941, September 2002. 22

M. Matsumoto and H. Kubotani. A statistical test for correlation between crater formation rate and mass extinctions. MNRAS, 282:1407–1412, October 1996. 4

A. Morbidelli. Chaotic Diffusion and the Origin of Comets from the 2/3 Resonance in the Kuiper Belt. *Icarus*, 127:1–12, May 1997. 12

A. Morbidelli and B. Gladman. Orbital and temporal distributions of meteorites originating in the asteroid belt. *Meteoritics and Planetary Science*, 33:999–1016, September 1998. 12

W. M. Napier. Evidence for cometary bombardment episodes. MNRAS, 366: 977–982, March 2006. 2, 12

G. Neukum and B. A. Ivanov. Crater Size Distributions and Impact Probabilities on Earth from Lunar, Terrestrial-planet, and Asteroid Cratering Data. In T. Gehrels, M. S. Matthews, and A. M. Schumann, editors, *Hazards Due to Comets and Asteroids*, pages 359–+, 1994. 4, 5, 11, 39

Planetary and Space Science Centre. The Earth Impact Database. `http://www.unb.ca/passc/ImpactDatabase/`, 2006. Accessed: 14 Oct 2007. 49

M. R. Rampino and R. B. Stothers. Terrestrial mass extinctions, cometary impacts and the sun's motion perpendicular to the galactic plane. Nature, 308: 709–712, April 1984. 1, 11, 12

D. M. Raup and J. J. Sepkoski, Jr. Periodicity of extinctions in the geologic past. *Proceedings of the National Academy of Science*, 81:801–805, 1984. 1

R. D. Schwartz and P. B. James. Periodic mass extinctions and the sun's oscillation about the galactic plane. Nature, 308:712–+, April 1984. 1, 11

Siberian Center For Global Catastrophes. Catalogue of the Earth's Impact structures. `http://omzg.sscc.ru/impact/index1.html`, 2008. Accessed: 23 Feb 2008). 49

D. I. Steel, D. J. Asher, W. M. Napier, and S. V. M. Clube. Are Impacts Correlated in Time? In T. Gehrels, M. S. Matthews, and A. M. Schumann, editors, *Hazards Due to Comets and Asteroids*, pages 463–+, 1994. 12

R. B. Stothers. The period dichotomy in terrestrial impact crater ages. MNRAS, 365:178–180, January 2006. 2

J. S. Trefil and D. M. Raup. Numerical simulations and the problem of periodicity in the cratering record. *Earth and Planetary Science Letters*, 82:159–164, March 1987. 2, 11, 39

D. P. Whitmire and A. A. Jackson. Are periodic mass extinctions driven by a distant solar companion? Nature, 308:713–715, April 1984. 1, 11

Earl G. Williams. *Fourier Acoustics: Sound Radiation and Nearfield Acoustical Holography*, page 8. Academic Press, 1999. 15

Appendix A

Convolution of the even and Gaussian distributions

The first random variable x has an *even* distribution between a and b

$$g_1(x,a,b) = \begin{cases} 0, & x < a \\ \frac{1}{b-a,} & a \le x \le b \\ 0, & x > b \end{cases}$$

$$G_1(x,a,b) = \begin{cases} 0, & x < a \\ \frac{x-a}{b-a}, & a \le x \le b \\ 1, & x > b. \end{cases}$$

The second random variable y has a *normal* distribution with a mean μ and a standard deviation σ

$$\begin{aligned} g_2(y,\mu,\sigma) &= \frac{1}{\sigma\sqrt{2\pi}} \mathrm{e}^{-\frac{1}{2}\left(\frac{y-\mu}{\sigma}\right)^2} \\ G_2(y,\mu,\sigma) &= \frac{1}{\sigma\sqrt{2\pi}} \int_{-\infty}^{y} \mathrm{e}^{-\frac{1}{2}\left(\frac{t-\mu}{\sigma}\right)^2} dt. \end{aligned}$$

Note that for simplicity we use the notation σ here in the Appendix, while in the text this error is referred to as σ_P. The cumulative distribution function for the sum

$$z = x + y$$

is obtained from the convolution

$$G(z) = \int_{-\infty}^{\infty} G_1(z-x,a,b) g_2(x,\mu,\sigma) dx. \tag{A.1}$$

Because $g_2(x,\mu,\sigma) > 0$ for $\forall x$, the product $G_1(z-x,a,b)g_2(x,\mu,\sigma) \ge 0$ only when $G_1(z-x,a,b) \ge 0$. There are three cases

1. case: $G_1(z-x,a,b) = 0$ when $z - x < a \Leftrightarrow x > z - a$
2. case: $G_1(z-x,a,b) = \frac{z-x-a}{b-a}$ when $a \leq z - x \leq b \Leftrightarrow z - b \leq x \leq z - a$
3. case: $G_1(z-x,a,b) = 1$ when $z - x > b \Leftrightarrow x < z - b$.

The convolution integral in Eq. A.1 becomes

$$G(z) = \int_{-\infty}^{z-b} g_2(x,\mu,\sigma)dx + \int_{z-b}^{z-a} \frac{z-x-a}{b-a} g_2(x,\mu,\sigma)dx \qquad (A.2)$$
$$= I_0 + \frac{1}{b-a}\left(I_1 - I_2\right),$$

where the three integrals are

$$I_0 = \int_{-\infty}^{z-b} g_2(x,\mu,\sigma)dx = G_2(z-b,\mu,\sigma) \qquad (A.3)$$

$$I_1 = (z-a)\int_{z-b}^{z-a} g_2(x,\mu,\sigma)dx \qquad (A.4)$$
$$= (z-a)\left[G_2(z-a,\mu,\sigma) - G_2(z-b,\mu,\sigma)\right]$$

$$I_2 = \int_{z-b}^{z-a} x g_2(x,\mu,\sigma)dx. \qquad (A.5)$$

The derivative of the density function $g_2(x,\mu,\sigma)$ can be used to solve I_2.

$$\frac{d}{dx}[g_2(x,\mu,\sigma)] = \frac{d}{dx}\left[\frac{1}{\sigma\sqrt{2\pi}}\mathrm{e}^{-\frac{1}{2}\left(\frac{x-\mu}{\sigma}\right)^2}\right] \qquad (A.6)$$
$$= \frac{1}{\sigma\sqrt{2\pi}}\mathrm{e}^{-\frac{1}{2}\left(\frac{x-\mu}{\sigma}\right)^2}\frac{d}{dx}\left[-\frac{1}{2}\left(\frac{x-\mu}{\sigma}\right)^2\right]$$
$$= -g_2(x,\mu,\sigma)\left(\frac{x-\mu}{\sigma}\right)\frac{1}{\sigma}$$
$$\Leftrightarrow x g_2(x,\mu,\sigma) = \mu g_2(x,\mu,\sigma) - \sigma^2\frac{d}{dx}[g_2(x,\mu,\sigma)]$$

Inserting this relation into Eq. A.5 gives

$$I_2 = \int_{z-b}^{z-a}\left[\mu g_2(x,\mu,\sigma) - \sigma^2\frac{d}{dx}[g_2(x,\mu,\sigma)]\right]$$
$$= \mu[G_2(z-a,\mu,\sigma) - G_2(z-b,\mu,\sigma)] -$$
$$\sigma^2[g_2(z-a,\mu,\sigma) - g_2(z-b,\mu,\sigma)] \qquad (A.7)$$

The solution for the integral in Eq. A.3 is now obtained from the I_0, I_1 and I_2 solutions (Eqs. A.3, A.5 and A.7)

$$G(z) = G_2(z-b,\mu,\sigma)$$
$$+ \frac{1}{b-a}\{(z-a-\mu)\left[G_2(z-a,\mu,\sigma) - G_2(z-b,\mu,\sigma)\right]$$
$$+ \sigma^2\left[g_2(z-a,\mu,\sigma) - g_2(z-b,\mu,\sigma)\right]\}. \qquad (A.8)$$

The density function for $z = x + y$ is obtained from the convolution

$$g(z) = \int_{-\infty}^{\infty} g_1(z - x, a, b) g_2(x, \mu, \sigma) dx. \tag{A.9}$$

Because $g_2(x, \mu, \sigma) > 0$ for $\forall x$, the product $g_1(z - x, a, b) g_2(x, \mu, \sigma) \geq 0$ only when $g_1(z - x, a, b) \geq 0$. Again, there are three cases

1. case: $g_1(z - x, a, b) = 0$ when $z - x < a \Leftrightarrow x > z - a$
2. case: $g_1(z - x, a, b) = \frac{1}{b-a}$ when $a \leq z - x \leq b \Leftrightarrow z - b \leq x \leq z - a$
3. case: $g_1(z - x, a, b) = 0$ when $z - x > b \Leftrightarrow x < z - b$.

Therefore the integral in Eq. A.9 becomes

$$\begin{aligned} g(z) &= \int_{z-b}^{z-a} \frac{1}{b-a} g_2(x, \mu, \sigma) dx \qquad (A.10) \\ &= \frac{1}{b-a} \left[G_2(z - a, \mu, \sigma) - G_2(z - b, \mu, \sigma) \right]. \end{aligned}$$

Finally, we can check that the results in Eqs. A.8 and A.11, because the correct results should fulfill the relation

$$\frac{dG(z)}{dz} = g(z). \tag{A.11}$$

But before solving the derivative of $G(z)$, the relation in Eq. A.7 rewritten into the form:

$$x g_2(x, \mu, \sigma) - \mu g_2(x, \mu, \sigma) + \sigma^2 \frac{d}{dx} [g_2(x, \mu, \sigma)] = 0.$$

This gives the following two useful relations

$$\begin{aligned} (z - a) g_2(z - a, \mu, \sigma) - \mu g_2(z - a, \mu, \sigma) + \sigma^2 \frac{d}{dx} [g_2(z - a, \mu, \sigma)] &= 0 \\ -(z - b) g_2(z - b, \mu, \sigma) + \mu g_2(z - b, \mu, \sigma) - \sigma^2 \frac{d}{dx} [g_2(z - b, \mu, \sigma)] &= 0. \end{aligned}$$

The sum of the terms underlined on each line below is zero:

$$\begin{aligned}
\tfrac{dG(z)}{dz} &= \\
\tfrac{dG_2(z-b,\mu,\sigma)}{dz} &+ \tfrac{1}{b-a}\left\{[G_2(z-a,\mu,\sigma)-G_2(z-b,\mu,\sigma)]+(z-a-\mu)\left[\tfrac{dG_2(z-a,\mu,\sigma)}{dz}-\tfrac{dG_2(z-b,\mu,\sigma)}{dz}\right]+\sigma^2\left[\tfrac{dg_2(z-a,\mu,\sigma)}{dz}-\tfrac{dg_2(z-b,\mu,\sigma)}{dz}\right]\right\} = \\
g_2(z-b,\mu,\sigma) &+ \tfrac{1}{b-a}\left\{[G_2(z-a,\mu,\sigma)-G_2(z-b,\mu,\sigma)]+(z-a-\mu)\,[g_2(z-a,\mu,\sigma)-g_2(z-b,\mu,\sigma)]+\sigma^2\left[\tfrac{dg_2(z-a,\mu,\sigma)}{dz}-\tfrac{dg_2(z-b,\mu,\sigma)}{dz}\right]\right\} = \\
g_2(z-b,\mu,\sigma) &+ \tfrac{1}{b-a}\,[G_2(z-a,\mu,\sigma)-G_2(z-b,\mu,\sigma)]+ \\
&\quad \tfrac{1}{b-a}\left\{\underline{\underline{(z-a)g_2(z-a,\mu,\sigma)}}-(z-a)g_2(z-b,\mu,\sigma)\underline{\underline{-\mu g_2(z-a,\mu,\sigma)}}+\mu g_2(z-b,\mu,\sigma)\underline{\underline{+\sigma^2\tfrac{dg_2(z-a,\mu,\sigma)}{dz}}}-\sigma^2\tfrac{dg_2(z-b,\mu,\sigma)}{dz}\right\} = \\
g_2(z-b,\mu,\sigma) &+ \tfrac{1}{b-a}\,[G_2(z-a,\mu,\sigma)-G_2(z-b,\mu,\sigma)]+\tfrac{1}{b-a}\left\{-(z\underline{\underline{-b+b}}-a)g_2(z-b,\mu,\sigma)+\mu g_2(z-b,\mu,\sigma)-\sigma^2\tfrac{dg_2(z-b,\mu,\sigma)}{dz}\right\} = \\
g_2(z-b,\mu,\sigma) &+ \tfrac{1}{b-a}\,[G_2(z-a,\mu,\sigma)-G_2(z-b,\mu,\sigma)]+\tfrac{1}{b-a}\left\{\underline{\underline{-(b-a)g_2(z-b,\mu,\sigma)-(z-b)g_2(z-b,\mu,\sigma)+\mu g_2(z-b,\mu,\sigma)-\sigma^2\tfrac{dg_2(z-b,\mu,\sigma)}{dz}}}\right\} = \\
\underline{\underline{g_2(z-b,\mu,\sigma)}} &+ \tfrac{1}{b-a}\,[G_2(z-a,\mu,\sigma)-G_2(z-b,\mu,\sigma)]\underline{\underline{-g_2(z-b,\mu,\sigma)}} = g(z)
\end{aligned}$$

The connection between Eqs. A.8, A.11 and A.11 has now been verified. In other words, our results for $G(z)$ and $g(z)$ are certainly correct.
Using the following connections

$$f_2(t, a_k, b_k) \equiv g_1(x, a, b)$$

$$F_2(t, a_k, b_k) \equiv G_1(x, a, b)$$

$$f_G(t, \mu, \sigma) \equiv g_2(y, \mu, \sigma)$$

$$F_G(t, \mu, \sigma) \equiv G_2(y, \mu, \sigma)$$

we can solve the convolution of $f_A(t)$ and $F_A(t)$ (Eqs. 6.3 and 6.5) with $f_G(t, \mu, \sigma)$ and $F_G(t, \mu, \sigma)$ (Eqs. 5.1 and 5.2). The probability density function is

$$f_A(t) = \sum_{k=1}^{K} \frac{A_k}{b_k - a_k} \left[F_G(t - a_k, \mu, \sigma) - F_G(t - b_k, \mu, \sigma) \right].$$

Using the following relations

$$a_k = k - 1$$

$$b_k = k$$

$$\mu = 0$$

$$F_G(t - a_k, \mu = 0, \sigma) = F_G(t, \mu = a_k, \sigma) = F_G(t, a_k, \sigma) = F_G(t, k - 1, \sigma)$$

$$F_G(t - b_k, \mu = 0, \sigma) = F_G(t, \mu = b_k, \sigma) = F_G(t, b_k, \sigma) = F_G(t, k, \sigma)$$

gives the final form

$$f_A(t, \sigma) = \sum_{k=1}^{K} A_k \left[F_G(t, k - 1, \sigma) - F_G(t, k, \sigma) \right]. \tag{A.12}$$

The cumulative distribution function is

$$\begin{aligned} F_A(t, \sigma) &= \sum_{k=1}^{K} A_k F_G(t - b_k, \mu, \sigma) \\ &+ \frac{A_k}{b_k - a_k} \{ (t - a_k - \mu) \left[F_G(t - a_k, \mu, \sigma) - F_G(t - b_k, \mu, \sigma) \right] \\ &+ \sigma^2 \left[f_G(t - a_k, \mu, \sigma) - f_G(t - b_k, \mu, \sigma) \right] \}. \end{aligned}$$

Using the following two additional relations

$$f_G(t - a_k, \mu = 0, \sigma) = f_G(t, \mu = a_k, \sigma) = f_G(t, a_k, \sigma) = f_G(t, k - 1, \sigma)$$

$$f_G(t - b_k, \mu = 0, \sigma) = f_G(t, \mu = b_k, \sigma) = f_G(t, b_k, \sigma) = f_G(t, k, \sigma)$$

gives the final form

$$\begin{aligned} F_A(t) &= \sum_{k=1}^{K} A_k \{ F_G(t, k, \sigma) \\ &+ (t - k + 1) \left[F_G(t, k - 1, \sigma) - F_G(t, k, \sigma) \right] \\ &+ \sigma^2 \left[f_G(t, k - 1, \sigma) - f_G(t, k, \sigma) \right] \} \end{aligned} \tag{A.13}$$

Appendix B

Recent impact crater data

Two comprehensive lists of terrestrial impact craters are maintained: the *The Earth Impact Database* (Planetary and Space Science Centre, 2006) and the *Catalogue of the Earth's Impact structures* (Siberian Center For Global Catastrophes, 2008). Here we study only *The Earth Impact Database*, because it has been used in previous studies (e.g. Jetsu, 1997; Jetsu and Pelt, 2000).

The *The Earth Impact Database* contains 174 impact crater records. When we select from these data only craters that have age and age error estimates that fulfil either criterion C_2 or C_3, we obtain two sub-samples of impact crater data presented in Table B.1. These contain $n = 38$ craters for C_2 and $n = 45$ for C_3. When these new revised records are compared to the data used in Jetsu (1997) we can conclude that the number of known impact craters has increased somewhat over the years. With C_2 the increase is only four craters (≈ 10 %) while with C_3 the change is 10 craters (≈ 22 %).

The uncertainty in these re-examined crater ages was analyzed as already done to the old crater ages in Chapter 3. The whole time span between the youngest and the oldest impact crater was divided into ten equal length time intervals or periods P_K. For each crater the uncertainty σ_P relative to this period was calculated as in Eq. 3.2 and finally the individual uncertainties were averaged into $\bar{\sigma_P}$. These values of σ_P are shown in Table B.1. The average age uncertainty $\bar{\sigma_p}$ for C_2 is 0.160 and that for C_3 0.193. When these inaccuracies are compared to the inaccuracies 0.170 for C_2 and 0.202 for C_3 in Jetsu (1997), we can note that the mean accuracy of the *The Earth Impact Database* data has improved by approximately 5 %. It should be emphasized, however, that in many cases the crater ages in the latest revisited data does not even fit inside the error estimates of the same ages in the earlier data in Table 2.1. For example, the older age estimate for Boltysh in Ukraine was 88 ± 3 million years, while the more recent data gives the re-evaluated value of 65.17 ± 0.64 million years. This, along with the fact that the sub-sample selection criteria have a significant effect

on the average error of the crater ages, could indicate that the actual crater age inaccuracies are far greater than the ones presented in the impact crater database. This is further supported by Deutsch and Schaerer (1994), who conclude that "an unsatisfactory situation exists in the error assignment to [crater] ages, because quoted uncertainties frequently reflect internal precision only, yielding unrealistically small errors".

Table B.1: Terrestrial impact crater data from *The Earth Impact Database*: name, location, diameter ($[D]$ = km), age ($[t]$ = My), age uncertainty ($[\sigma_t]$ = My), period length P_K calculated for C_2, period length P_K calculated for C_3, σ_P for C_2 and σ_P for C_3. The sub-samples are chosen with the criterion C_2 and C_3 in Jetsu (1997). Last row contains the average uncertainties $\bar{\sigma_P}$ for both sub-samples.

Crater	location	D	t	σ_t	P_{K,C_2}	P_{K,C_3}	σ_p for C_2	σ_p for C_3
Zhamanshin	Kazakhstan	14	0.9	0.1	24.35	-	0.0041	-
El'gygytgyn	Russia	18	3.5	0.5	24.35	-	0.0205	-
Karla	Russia	10	5	1	24.35	28.5	0.0411	0.0351
Bigach	Kazakhstan	8	5	3	24.35	28.5	0.1232	0.1053
Steinheim	Germany	3.8	15	1	-	28.5	0.0000	0.0351
Ries	Germany	24	15.1	0.1	24.35	28.5	0.0041	0.0035
Mien	Sweden	9	21	2.3	24.35	28.5	0.0945	0.0807
Chesapeake Bay	USA	90	35.5	0.3	24.35	28.5	0.0123	0.0105
Popigai	Russia	100	35.7	0.2	24.35	28.5	0.0082	0.0070
Mistastin	Canada	28	36.4	4	24.35	28.5	0.1643	0.1404
Wanapitei	Canada	7.5	37.2	1.2	24.35	28.5	0.0493	0.0421
Logancha	Russia	20	40	20	24.35	28.5	0.8214	0.7018
Beyenchime-Salaatin	Russia	8	40	20	24.35	28.5	0.8214	0.7018
Logoisk	Belarus	15	42.3	1.1	24.35	28.5	0.0452	0.0386
Shunak	Kazakhstan	2.8	45	10	-	28.5	-	0.3509
Ragozinka	Russia	9	46	3	24.35	28.5	0.1232	0.1053
Chiyli	Kazakhstan	5.5	46	7	24.35	28.5	0.2875	0.2456
Gusev	Russia	3	49	0.2	-	28.5	-	0.0070
Kamensk	Russia	25	49	0.2	24.35	28.5	0.0082	0.0070
Montagnais	Canada	45	50.5	0.76	24.35	28.5	0.0312	0.0267
Marquez	USA	12.7	58	2	24.35	28.5	0.0821	0.0702
Chicxulub	Mexico	170	64.98	0.05	24.35	28.5	0.0021	0.0018
Boltysh	Ukraine	24	65.17	0.64	24.35	28.5	0.0263	0.0225
Kara	Russia	65	70.3	2.2	24.35	28.5	0.0903	0.0772
Lappajärvi	Finland	23	73.3	5.3	24.35	28.5	0.2177	0.1860
Manson	USA	35	73.8	0.3	24.35	28.5	0.0123	0.0105
Zeleny Gai	Ukraine	3.5	80	20	24.35	28.5	0.8214	0.7018
Wetumpka	USA	6.5	81	1.5	24.35	28.5	0.0616	0.0526
Dellen	Sweden	19	89	2.7	24.35	28.5	0.1109	0.0947
Steen River	Canada	25	91	7	24.35	28.5	0.2875	0.2456
Deep Bay	Canada	13	99	4	24.35	28.5	0.1643	0.1404
Carswell	Canada	39	115	10	24.35	28.5	0.4107	0.3509
Rotmistrovka	Ukraine	2.7	120	10	-	28.5	-	0.3509
Tookoonooka	Australia	55	128	5	24.35	28.5	0.2053	0.1754
Mjølnir	Norway	40	142	2.6	24.35	28.5	0.1068	0.0912
Gosses Bluff	Australia	22	142.5	0.8	24.35	28.5	0.0329	0.0281
Morokweng	South Africa	70	145	0.8	24.35	28.5	0.0329	0.0281
Tabun-Khara-Obo	Mongolia	1.3	150	20	-	28.5	-	0.7018
Zapadnaya	Ukraine	3.2	165	5	-	28.5	-	0.1754
Puchezh-Katunki	Russia	80	167	3	24.35	28.5	0.1232	0.1053
Obolon'	Ukraine	20	169	7	24.35	28.5	0.2875	0.2456
Viewfield	Canada	2.5	190	20	-	28.5	-	0.7018
Manicouagan	Canada	100	214	1	24.35	28.5	0.0411	0.0351
Rochechouart	France	23	214	8	24.35	28.5	0.3285	0.2807
Araguainha	Brazil	40	244.4	3.25	24.35	28.5	0.1335	0.1140
Ternovka	Ukraine	11	280	10	-	28.5	-	0.3509
Clearwater East/West	Canada	36	290	20	-	28.5	-	0.7018
				$\bar{\sigma_p}$ for C_2 and C_3			*0.1600*	*0.1930*